Bioactive Materials 39 (2024) 595–611

Contents lists available at ScienceDirect

Bioactive Materials

journal homepage: www.keaipublishing.com/en/journals/bioactive-materials

Self-assembled carbon monoxide nanogenerators managing sepsis through scavenging multiple inflammatory mediators

Yang Wu [a,b,c,1], Xia Chen [a,d,1], Zhaolin Zeng [e], Bei Chen [a], Zhenxing Wang [a,b,c], Zhiyong Song [f], Hui Xie [a,b,c,*]

[a] Department of Orthopedics, Movement System Injury and Repair Research Center, Xiangya Hospital, Central South University, Changsha, Hunan, 410008, China
[b] Hunan Key Laboratory of Ângmedicine, Xiangya Hospital, Central South University, Changsha, Hunan, 410008, China
[c] National Clinical Research Center for Geriatric Disorders, Xiangya Hospital, Central South University, Changsha, Hunan, 410008, China
[d] Department of Clinical Laboratory, Xiangya Hospital, Central South University, Changsha, Hunan, 410008, China
[e] Department of Metabolism and Endocrinology, The First Affiliated Hospital, Hengyang Medical School, University of South China, Hengyang, Hunan, 421001, China
[f] State Key Laboratory of Agriculture Microbiology, College of Science, Huazhong Agricultural University, Wuhan, Hubei, 430070, China

ARTICLE INFO

Keywords:
Sepsis
Carbon monoxide nanogenerator
Heme oxygenase-1
Scavenging inflammatory storm

ABSTRACT

Sepsis, a life-threatening syndrome of organ damage resulting from dysregulated inflammatory response, is distinguished by overexpression of inflammatory cytokines, excessive generation of reactive oxygen/nitrogen species (RONS), heightened activation of pyroptosis, and suppression of autophagy. However, current clinical symptomatic supportive treatment has failed to reduce the high mortality. Herein, we developed self-assembled multifunctional carbon monoxide nanogenerators (Nano CO), as sepsis drug candidates, which can release CO in response to ROS, resulting in clearing bacteria and activating the heme oxygenase-1/CO system. This activation strengthened endogenous protection and scavenged multiple inflammatory mediators to alleviate the cytokine storm, including scavenging RONS and cfDNA, inhibiting macrophage activation, blocking pyroptosis and activating autophagy. Animal experiments show that Nano CO has a good therapeutic effect on mice with LPS-induced sepsis, which is manifested in hypothermia recovery, organ damage repair, and a 50% decrease in mortality rates. Taken together, these results illustrated the efficacy of multifunctional Nano CO to target clearance of multiple mediators in sepsis treatment and act against other refractory inflammation-related diseases.

1. Introduction

The third edition of the International Consensus Definition of Sepsis (Sepsis 3.0) characterizes sepsis as a clinical syndrome marked by dysregulated inflammatory response caused by various pathogens, including bacteria, viruses, fungi and other pathogens, ultimately resulting in physiological and organ dysfunction [1,2]. Sepsis affects millions of patients globally each year, with a mortality rate exceeding 25%, making it a leading causes of death in intensive care units (ICUs) [3]. Current clinical treatment primarily focus on symptomatic supportive measures, predominantly involving antibiotics, antagonists, and supportive nursing [4]. However, such goal-oriented approach has not significantly improved the cure and survival rate of critically ill patients [5]. It is noteworthy that approximately 40% of sepsis patients experience re-hospitalization within three months post-discharge. This phenomenon is primarily attributed to residual inflammatory mediators in the body, provoking a second cytokine storm [3,6]. Consequently, the unpredictable, dynamic and uncontrollable inflammatory response in patients presents a huge challenge to sepsis treatment.

In a septic state, the dysregulation of inflammatory is often triggered by overactivation of toll-like receptors (TLRs), which can recognize multiple inflammatory mediators such as lipopolysaccharide (LPS) [7], reactive oxygen/nitrogen species (RONS) [8] and cell-free DNA (cfDNA) [9], thereby inducing the release of inflammatory cytokines and nitric

Peer review under responsibility of KeAi Communications Co., Ltd.
* Corresponding author. Department of Orthopedics, Movement System Injury and Repair Research Center, Xiangya Hospital, Central South University, Changsha, Hunan, 410008, China.
E-mail address: huixie@csu.edu.cn (H. Xie).
[1] These authors contributed equally to this work.

https://doi.org/10.1016/j.bioactmat.2024.04.013
Received 9 January 2024; Received in revised form 29 March 2024; Accepted 14 April 2024

oxide (NO) [10]. These circulating inflammatory mediators perpetuated systemic inflammation, resulting in cell damage, organ failure and potential mortality. Therefore, we speculated that reducing ROS levels and removing various inflammatory mediators were crucial aspects of sepsis treatment. In the progression of sepsis, pyroptosis, a pro-inflammatory programmed cell death mechanism, is triggered by factors including infection and injury-related signals. This process leads to the release of a significant quantity of cytokines through plasma membrane rupture, contributing to cell death and accelerating the advancement of sepsis [11,12]. Simultaneously, autophagy, the second programmed cell death mode, is inhibited, resulting in dysregulated inflammatory responses and hindered clearance of damaged cells, ultimately affecting the function of vital organs [10,13]. Consequently, blocking pyroptosis and activating autophagy has emerged as an additional therapeutic target for sepsis, which was conducive to cell repair and survival, even protected tissue and organ from damage. Hence, addressing the complex physiological and pathological state of sepsis necessitated the development of pharmacological intervention that can act simultaneously on multiple targets, thereby efficiently controlling sepsis.

Carbon monoxide (CO) serves as a pivotal molecule in cellular protection and homeostasis, exhibiting crucial signaling capabilities under both physiological and pathophysiological conditions. It plays a vital role in regulating stress responses and cellular adaptation to injury [14–16]. Heme Oxygenase-1 (HO-1) and its catalytic product, CO, significantly contribute to endogenous protective mechanisms aganist cellular stress, participating in the regulation of oxidative stress, inflammation, autophagy, pyroptosis and other pathophysiological processes [17–19]. Consequently, the exogenous delivery of CO can trigger a cascade of cellular protection mechanisms during stress and inflammation, activating essential endogenous defense functions [20–22]. Additionally, it is worth noting that CO is a non-radical group and poses no toxic side effects at low doses, making it an ideal gas molecule for sepsis treatment [23]. However, the existing CO precursor drugs frequently face challenges related to poor water solubility, uncontrollable dosage, and potential toxicity [24–26]. Addressing these obstacles is a crucial aspect of our research endeavor.

Herein, we applied nano-self-assembly technology to construct injectable CO nanodrugs for treating sepsis, capable of releasing CO in response to ROS within the body. We proposed an instructive schematic diagram outlining the design of polysulfhydrylated polyesters and diiron nonacarbonyl as the key nanocomponents of CO nanogenerators (Nano CO) (Scheme 1). Moreover, we delved into the anti-sepsis activity of Nano CO through investigations in cell models and animal models, focusing on six beneficial therapeutic mechanisms: (1) antibacterial

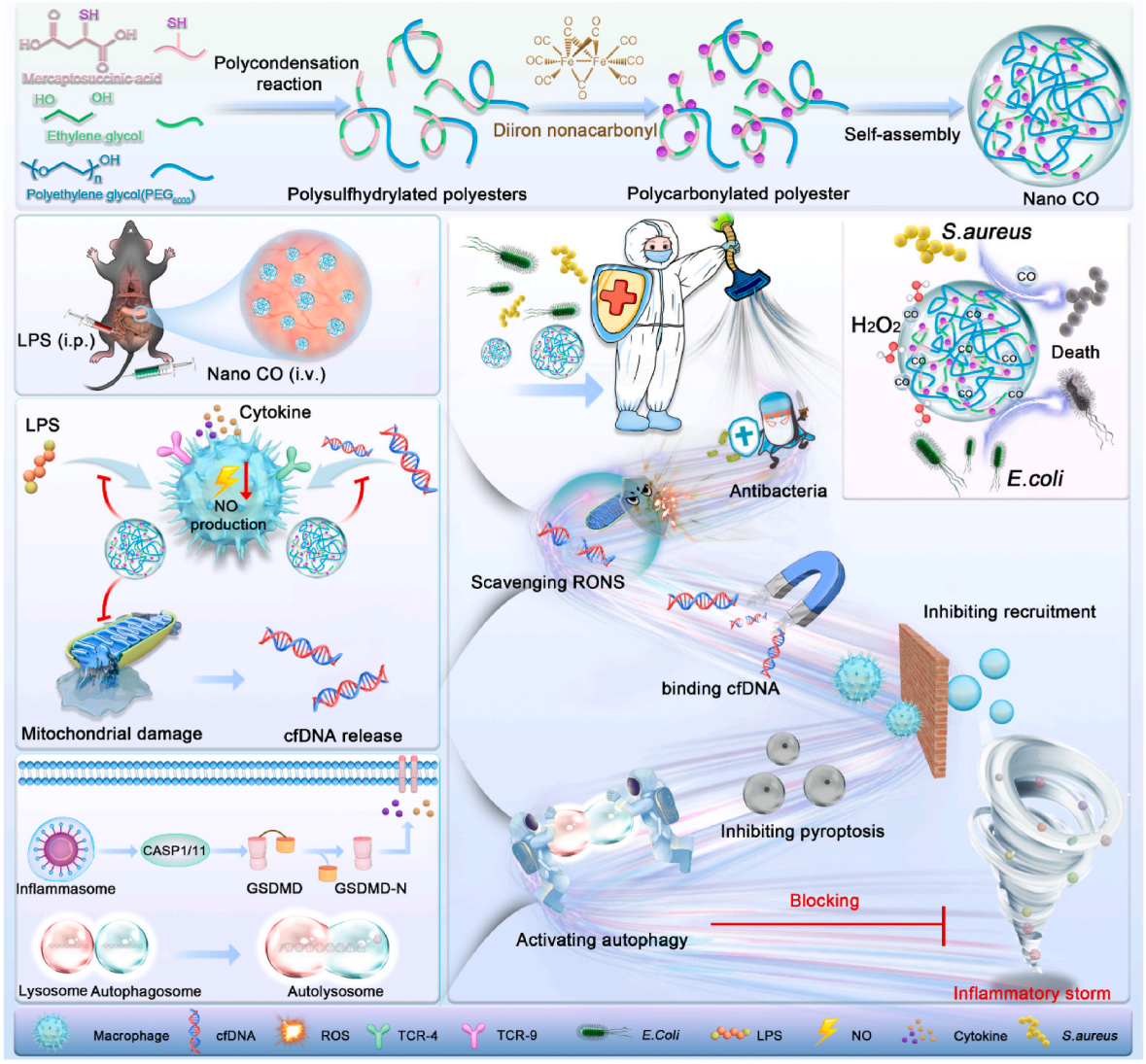

Scheme 1. Schematic diagram of the design of self-assembled Nano CO and its ability to clear multiple inflammatory mediators in sepsis. (1) antibacterial and inhibiting LPS-induced NO production; (2) scavenging of RONS (•OH, $•O_2^-$ and •NO) and inhibiting oxidative stress-induced DNA damage and cell death; (3) binding and clearance of cfDNA; (4) blocking activated macrophage recruitment; (5) inhibiting pyroptosis; (6) inducing autophagy.

effects and inhibition of LPS-induced NO production; (2) scavenging of RONS (•OH, $•O_2^-$ and •NO) and inhibiting oxidative stress-induced DNA damage and cell death; (3) binding and clearance of cfDNA; (4) blocking activated macrophage recruitment. Surprisingly, Nano CO could effectively (5) inhibit pyroptosis, and (6) induce autophagy. We proposed that this multifunctional nanomaterial could serve as an ideal therapeutic options in combating sepsis, given its diverse and potent mechanisms of action.

2. Materials and methods

2.1. Synthesis and preparation of the Nano CO

In brief, ethylene glycol (6.6 mmol), mercaptosuccinic acid (6.6 mmol) and mPEG-OH (0.4 mmol, Mn = 4000) were added into a reaction flask with p-toluenesulfonic acid (0.84 mmol) and EDTA (0.54 mmol) as the catalyst. The reaction was carried out under the nitrogen atmosphere for 8 h at 120 °C. Then, the product was dissolved in acetone and precipitated in diethyl ether three times to obtain polysulfhydrylated polyesters (PSP).

Then, diiron nonacarbonyl (50 mg) and PSP (200 mg) were dissolved in 50 mL THF and stirred in nitrogen at 50 °C for 2 h. The solution turned brown and cooled to −20 °C at the end of the reaction. n-Hexane was added to the cold solution to obtain brown precipitation. The precipitate was further washed with diethyl ether and dried to obtain brown solid polycarbonyl polyester. Finally, the obtained polycarbonyl polyester was stored at −4 °C for further use. The resulting polymer was self-assembled into Nano CO in deionized water after ultrasound at 0 °C for 10 min.

2.2. CO release assay

The released CO in PBS was detected spectrophotometrically by measuring the conversion of hemoglobin (Hb) to carboxyhemoglobin (HbCO). First, bovine hemoglobin (5.5 μM) was completely dissolved in PBS, and then reduced by adding SDT (1.5 mg) under N_2 atmosphere. Nano CO (50 μL, 5 mg/mL) was added into the above 4 mL solution and the absorption spectrum of the solution (375–475 nm) was detected at interval 10 min. In order to eliminate influencing factors and enhance the accuracy, two strong adsorption bands at 410 nm and 430 nm (attributed to HbCO and Hb, respectively) were used to quantify the conversion of Hb to HbCO. The Beer-Lambert law was used to calculate the Hb-to-HbCO conversion percentage (x) and the concentration of released CO which was coordinated with Hb, as indicated by following Equation (1).

$$C_{CO} = C_{Hb} \times x = \frac{528.6 \times A_{410nm} - 304 \times A_{430nm}}{216.5 \times A_{410nm} + 442.4 \times A_{430nm}} C_{Hb} \quad 1$$

2.3. DPPH free radical scavenging activity

Different concentration of Nano CO or PSP solution were added to 200 mM $DPPH^•$ ethanol solution and vortexed mixing. The UV absorbance spectrum of the mixed solution (from 300 to 700 nm) was measured at 5 min interval. A standard curve was prepared to quantify $DPPH^•$ at 517 nm, from which the $DPPH^•$ scavenging percentage in the presence of various concentrations of Nano CO or PSP was calculated.

2.4. ABTS free radical scavenging activity

$ABTS^{+•}$ working solution was prepared by mixing ABTS (0.74 mM) with $(NH_4)_2S_2O_8$ (0.26 mM) (1:1, v/v) and storing at 4 °C overnight in the dark. Then, the different concentration of Nano CO or PSP solution were added to the above solution and vortexed mixing. The UV spectra from 400 to 850 nm of the mixed solution was recorded at 5 min interval. Similarly, the $ABTS^{+•}$ scavenging percentage was calculated based on $ABTS^{+•}$ standard curve.

2.5. ROS scavenging activity

The ROS scavenging activity of Nano CO was measured by Hydroxyl free radical assay kit (Jiancheng, Nanjing, China) and Micro Superoxide Anion Assay Kit (Abbkine, Wuhan, China). Briefly, $FeSO_4$ solution (10 mM) reacted with 1% H_2O_2 (5 μL) to generate •OH, while xanthine (5 μL, 560 mM) and xanthine oxidase (5 μL, 1:10 dilution) were mixed to produce $•O_2^-$. Different concentrations of Nano CO or PSP were rapidly added to above solution, respectively. Then, the •OH and $•O_2^-$ working solution were added to the above mixed solution and the absorption spectrum of 400–700 nm was recorded.

2.6. RNS scavenging activity

The RNS scavenging activity was measured by Nitric oxide detection kit (Beyotine, Shanghai, China). Briefly, SNP (100 μL, 20 mM), as •NO donor, were mixed with different concentration of Nano CO or PSP (100 μL) in of PBS solution (200 μL, 0.2 M, pH 7.4), and then shaken at 37 °C. After the reaction, Griess reagent were added for detect the UV spectra of 400–700 nm.

2.7. Intracellular RONS scavenging activity

RAW264.7 cells were seeded on coverslips in 12-well plates and cultured overnight (37 °C, 5% CO_2). The cells were then treated with 10 μg/mL LPS for 24 h, with blank medium as a control. Next, LPS-treated cells were incubated with Nano CO or PSP (200 μg/mL) for an additional 24 h. Subsequently, different types of oxidative stress probes (DCFH-DA for ROS, dihydroethidium for $•O_2^-$ and DAF-FM DA for •NO) were added for staining for 30 min and blocked with DAPI. Intracellular RONS levels were finally observed by fluorescence microscopy (Zeiss, Germany). To quantify the RONS level, the same treatments cells were harvested, and the fluorescence intensity was measured by BD FACSAria Fusion cell analyzer (BD, USA).

2.8. Inhibition of LPS-induced nitric oxide generation

RAW264.7 cells were seeded on coverslips in 96-well plates and were allowed to adhere overnight in growth medium (37 °C, 5% CO_2). The cells were then treated with LPS (1 μg/mL), LPS (1 μg/mL) + PSP (200 μg/mL) and LPS (1 μg/mL) + Nano CO (200 μg/mL) for 24 h, respectively. The untreated cells served as a control group, and cells only treated with LPS as a positive group. Then the supernatants were collected and mixed with nitric oxide (NO) assay kit, and NO concentration was measured with a multiwell plate reader (Thermo Fisher, USA).

2.9. In vitro anti-macrophage migration activity

RAW264.7 cells were seeded on coverslips in 24-well plates and were allowed to adhere overnight in growth medium. The cells were treated with LPS (1 μg/mL) for 4 h. LPS-treated RAW264.7 cells were digested with pancreatic enzyme and centrifuged at 1500 rpm for 5min, then suspended in medium without FBS. 2×10^5 cells were transferred to transwell chambers, and incubated with Nano CO or PSP (200 μg/mL). Untreated cells were used as the control group, and cells treated only with LPS were used as the positive group. After migration for 24 h, cells on the upper side of each insert were gently removed with a cotton swab. Subsequently, the migrating cells on the lower side of each insert were fixed and stained with 0.5% crystal violet. Finally, the stained cells were imaged by microscope (Zeiss, Germany).

2.10. Antibacterial effect of Nano CO

Staphylococcus aureus (*S. aureus*) and *Escherichia coli* (*E. coli*) were inoculated into a 96-well plate at 10^6 CFU/mL, and the bacteria were treated with following protocols for 2 h, such as PBS, H_2O_2 (100 μM), PSP (200 μg/mL), Nano CO (200 μg/mL), Nano CO (200 μg/mL) + H_2O_2 (100 μM). Then, the optical density at 600 nm (OD600) of the bacteria was measured at 1 h interval. Next, we used the dilution plate method to evaluate the inhibitory effect of different concentrations of Nano CO (50, 100, 200 μg/mL) on bacteria with the assistance of H_2O_2. Briefly, *S. aureus* and *E. coli* were incubated with Nano CO with the assistance of H_2O_2 (100 μM) for 2 h. The number of bacteria was then counted by the plate method, and the antibacterial efficiency was calculated.

2.11. Inhibition of pyroptosis induced by canonical and noncanonical inflammasomes

First, prepare and culture primary mouse bone marrow-derived macrophages, and seed them into a 12-well plate (see Supporting Information for details) [27]. For canonical inflammasome activation (NLRP3), RAW264.7 were stimulated with LPS (100 ng/mL) for 4 h, then Nano CO with different concentrations (200, 100, 50 μg/mL) and ATP (3 mM) was added and incubated for 1 h. For noncanonical inflammasome activation, RAW 264.7 were treated with Pam3CSK4 (1 μg/mL) for 3 h to induce caspase-11 expression. Then Nano CO with different concentrations (200, 100, 50 μg/mL) and LPS (1 μg/mL) was added and incubated for 24 h. Next, the cell culture supernatant was collected to detect the release of LDH. Cells were stained with PI and imaged using fluorescence microscopy (Zeiss, Germany). After the same treatment as above, cells were collected to Weston-Blot analysis.

2.12. Inhibition of autophagy

Prepare and culture primary mouse bone marrow-derived macrophages, and seed them into a 12-well plate [27]. The cells are then treated for 24 h according to the established schedule, such as PBS, LPS (1 μg/mL), LPS (1 μg/mL) + Nano CO (200 μg/mL), LPS (1 μg/mL) + PSP (200 μg/mL). Then it was fixed with electron microscope fixative and TEM imaging was performed. On the other hand, after the same treatment, cells were collected and Weston-Blot was used to analyze the LC3 protein contents in the cells.

2.13. LPS-induced sepsis model

Male C57BL/6 mice were intravenously injected with LPS in different doses (30, 25, 20 and 15 mg/kg). Clinical scores, mortality and body weight were recorded for 7 consecutive days to further evaluate the half-lethal dose (LD50) of LPS. The criteria of clinical score were listed as follows: 0, no symptoms; 1, piloerection and huddling; 2, piloerection, diarrhea, and huddling; 3, lack of interest in surroundings and severe diarrhea; 4, decreased movement and listless appearance; 5, loss of self-righting reflex. Mice were euthanized when they exhibited a score of 5.

2.14. Treatment of LPS-induced sepsis mice

Male C57BL/6 mice were randomly divided into control group (PBS), positive group (LPS), LPS + PSP group and LPS + Nano CO group (n = 20). C57BL/6 mice were intravenously injected with PBS, PSP (30 mg/kg) or Nano CO (30 mg/kg) at 6 and 3 h before injected with a LD50 of LPS. The serum levels of HO-1, MDA, cfDNA, NO, TNF-α and IL-6 were measured 12 h after LPS challenge. The mice clinical scores, mortality, body temperature and body weight were recorded for 7 consecutive days.

2.15. Fraction of M1 polarized macrophages in peritoneal cavity

The fraction of M1 polarized macrophages in the peritoneal cavity was evaluated by flow cytometry. Briefly, a peritoneal lavage was performed with 5 mL of PBS containing 10% FBS, and the cells were collected and stained with APC anti-mouse CD86 antibodies, PerCP/Cy5.5 anti-mouse CD11b antibodies and FITC-anti-F4/80 antibodies at 4 °C for 1 h. After repeated washes with PBS, the cells were analyzed with a BD FACSAria Fusion cell analyzer (BD, USA). The CD11b, F4/80 and CD86 triple-positive cells represent the M1-polarized macrophages.

2.16. Fraction of cells with high ROS level in peritoneal cavity

Cells were collected by peritoneal lavage and were stained with DCFH-DA at 4 °C for 1 h. After repeated washes with PBS, the cells were analyzed with a BD FACSAria Fusion cell analyzer (BD, USA).

2.17. Histological analysis

The mouse tissues were fixed in 4% paraformaldehyde for 24 h and then sliced after paraffin embedding. The sections were prepared with standard procedures and then H&E staining, immunohistochemistry and immunofluorescence were performed.

2.18. Statistical analysis

All the results were presented as the mean value plus a standard deviation (±SD) from at least three independent experiments. Statistical analyses were performed using the *t*-test. Values of $^*p < 0.05$, $^{**}p < 0.01$, and $^{***}p < 0.001$ were considered statistically significant. All statistical analyses were performed with Origin software.

3. Results and discussion

3.1. Preparation and characterization of Nano CO

Nano CO were synthesized through polycondensation reaction involving mercaptosuccinic acid and ethylene glycol to obtain polysulfhydrylated polyesters (PSP) [28,29]. Then, diiron nonacarbonyl ($Fe_2(CO)_9$) was grafted onto the side chain of the PSP polymer to create polycarbonylated polyester, which underwent self-assembly at low temperature to obtain Nano CO (Fig. 1a) [30,31]. Gel Permeation Chromatography (GPC) testing revealed that PSP behaved as a single peak, showing an average molecular weight (Mw) of 11.70 kDa (Fig. 1b). Notably, the ^{1}H NMR spectrum displayed a distinct signal for thiol hydrogen at the 2.28 ppm, signifying the ideal stability of sulfhydryl group in the polycondensation process (Fig. S1). The successful grafting of Fe-CO groups onto polycarbonylated polyester was confirmed through Fourier Transform Infrared Spectrometer (FTIR). As illustrated in Fig. 1c, the polycarbonylated polyester exhibited characteristic infrared absorption peaks of carbonyl at 2077 cm^{-1} and 1085 cm^{-1}. Furthermore, the absorption peak observed in the range of 2800–3000 cm^{-1} represented the saturated C-H stretching vibration absorption peak associated with both polycarbonylated polyester and PSP. The ultraviolet (UV) absorption spectrum further confirmed that the characteristic absorption peak of polycarbonylated polyester at 330–340 nm belonged to the carbonyl group (Fig. 1d). Thermogravimetric analysis (TGA) demonstrated a carbon oxide loading capacity up to 15% (Fig. 1e). Subsequently, the prepared polymer underwent self-assembly into Nano CO via ultrasound at low temperature. Transmission electron microscopy (TEM) characterization revealed that Nano CO exhibited a uniform spherical morphology with excellent dispersion (Fig. 1f). Its size distribution was approximately 150 nm, consistent with the hydrated particle size (Fig. 1g). Moreover, regardless of the medium used PBS, DMEM, or a 10% FBS solution, the particle size of Nano CO remained stable over a prolonged period, highlighting its excellent

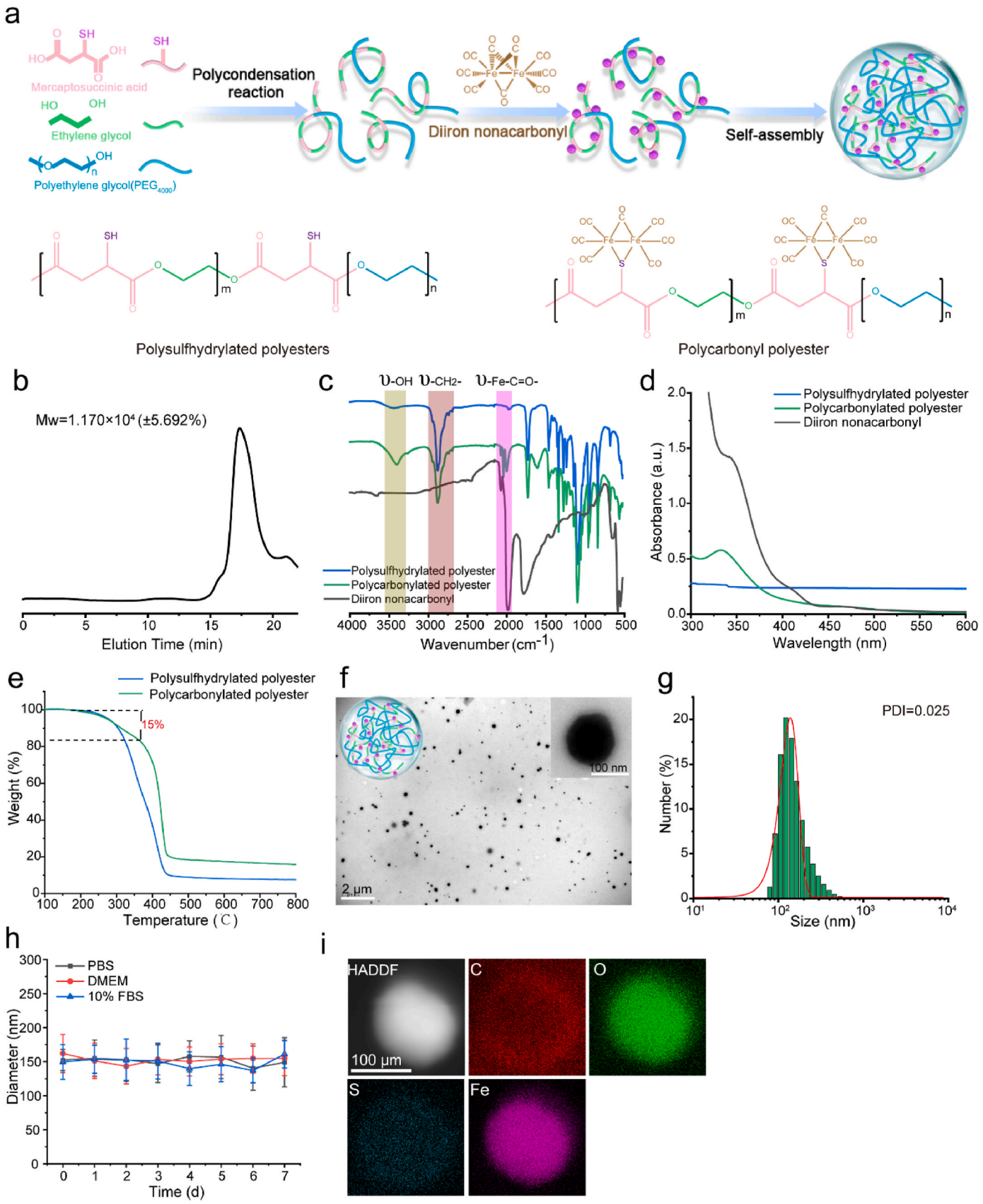

Fig. 1. Construction and characterization of Nano CO. (a) Schematic diagram of Nano CO synthesis. (b) GPC of polysulfhydrylated polyesters. (c) FT-IR spectra, (d) UV–vis absorption spectra and (e)TGA analysis of polysulfhydrylated polyesters, polycarbonylated polyester and diiron nonacarbonyl. (f) TEM image and (g) size distribution of Nano CO. (h) Particle size of Nano CO in different media, including PBS, DMEM, and 10% FBS solution. (i) Elemental mapping of Nano CO including C, O, S, and Fe elements.

stability (Fig. 1h). Furthermore, the element distribution diagram illustrated that the Fe, C, O and S elements were evenly distributed in the Nano CO, with Fe constituting 20.14% (Fig. 1i and Fig. S2). These characterization results underscored the successful synthesis of Nano CO and its commendable stability, thereby highlighting its potential therapeutic efficacy for sepsis.

Subsequently, as illustrated in schematic Fig. 2a, we evaluated the release kinetic behavior of Nano CO prodrug release dynamics in response to H_2O_2, simulating the microenvironment of ROS-rich cells or tissues in sepsis. Using hemoglobin (Hb) as the probe, the released CO concentration was measured by the UV method based on the absorption peaks of reduced Hb ($\lambda = 430$ nm) and HbCO ($\lambda = 410$ nm) [32,33]. As presented in Fig. 2b, Nano CO released CO in a concentration-dependent manner in the presence of H_2O_2. However, there was negligible release of Nano CO in an H_2O_2-free environment. Similarly, there was no release behavior of Nano CO in solutions with different pH values (pH = 5.0, 7.0 and 9.0) (Fig. S3a). The release of CO was also negligible in different media, including to 10% FBS, DMEM, and PBS (Fig. S3b). These findings highlighted the excellent stability of Nano CO across diverse environments. Overall, the facile polycondensation reaction, optimized CO storage and inflamed tissue-specific release made Nano CO ideal for treating septic reactions.

3.2. Antibacterial effect of Nano CO in vitro

Bacteria stand out as pivotal contributors to sepsis, with *Staphylococcus aureus* (*S. aureus*) and *Escherichia coli* (*E. coli*) being prominent pathogens. Rapid eradication of bacteria imperative for effective sepsis treatment. As depicted in Fig. 2c–d, Nano CO, assisted by H_2O_2, demonstrated the complete prevention of bacterial growth. However, both free Nano CO and PSP only resulted in a delay in bacterial growth without achieving complete inhibition. Next, we quantitatively evaluated the antimicrobial efficacy of Nano CO against *S. aureus* and *E. coli* when combined with H_2O_2. Nano CO exhibited concentration-dependent bacterial inhibition in the support of H_2O_2 (20 μM). At concentration of 200 μg/mL, the antibacterial efficiency of Nano CO against *S. aureus* and *E. coli* reached 97.93% and 97.81%, respectively (Fig. 2e–f). The schematic representation in Fig. 2g succinctly encapsulated these findings, emphasizing that Nano CO exhibited robust antibacterial effects under conditions favorable for CO release.

3.3. RONS scavenging activity of Nano CO

To evaluate the antioxidant capacity of Nano CO, we utilized two widely used commercial probes, namely $DPPH^{\bullet}$ and $ABTS^{+\bullet}$, to assess its free radical scavenging activity. After incubated with Nano CO solutions of different concentrations for 60 min, the color of the $DPPH^{\bullet}$ solution transitioned from purple to yellow, with the degree of change displaying a concentration-dependent increase (Fig. 3a). Importantly, even at a high concentration (200 μg/mL), PSP failed to induce any color change in the $DPPH^{\bullet}$ solution (Fig. S4). Catalytic kinetics calculations revealed that Nano CO (200 μg/mL) could eliminate 53.54% of the $DPPH^{\bullet}$ within 60 min (Fig. 3b). Similar observations were made with the $ABTS^{+\bullet}$ solution, which gradually turned colorless in a concentration-dependent manner after incubation with different concentrations of Nano CO (Fig. 3c). Notably, the color change in the $ABTS^{+\bullet}$ solution was

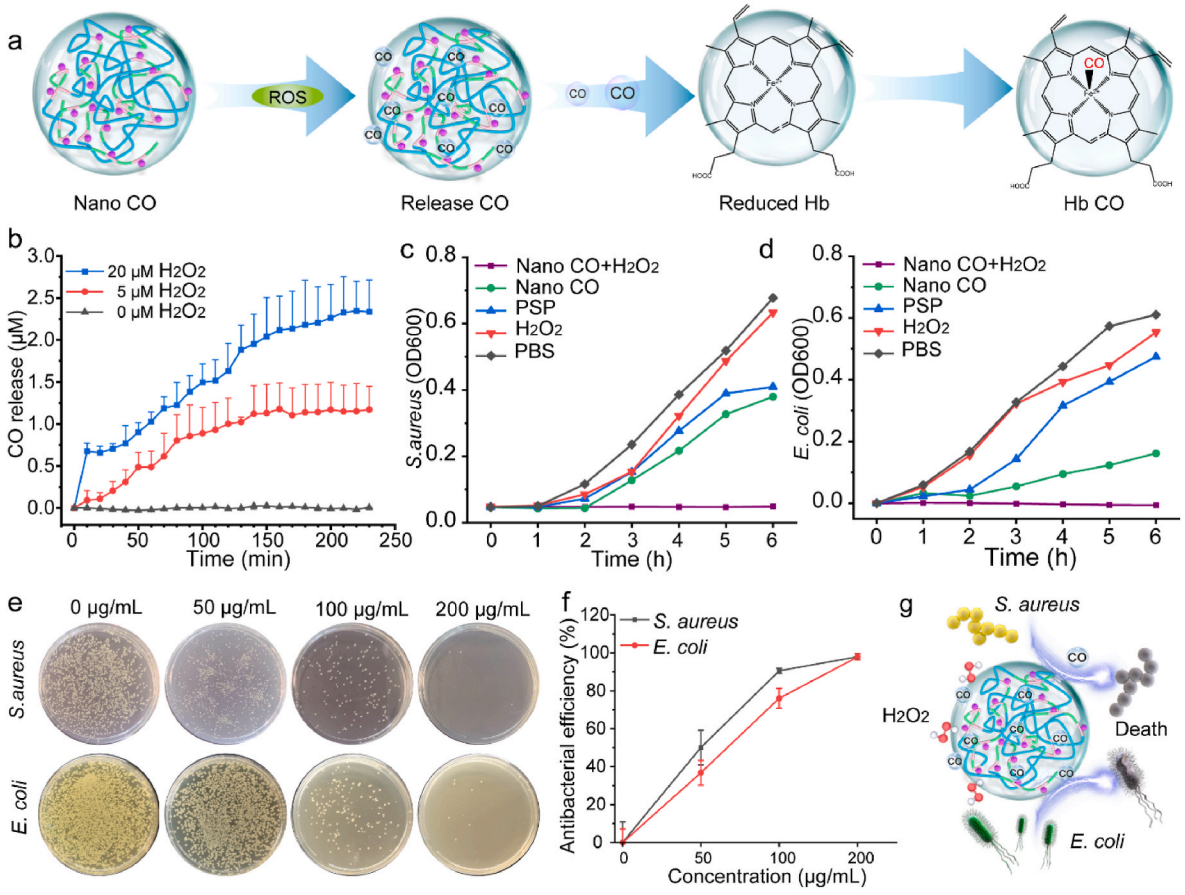

Fig. 2. Evaluation of releasing capacity and antibacterial effect of Nano CO. (a) Schematic diagram of CO release and detection. (b) CO release behavior of Nano CO under different concentrations of H_2O_2 (20, 5, 0 μM). (c–d) Growth curves of *S. aureus* and *E. coli* after different modes of action (PBS, 20 μM H_2O_2, 200 μg/mL PSP, 200 μg/mL Nano CO, 200 μg/mL Nano CO + 20 μM H_2O_2). (e–f) The antibacterial effect of Nano CO at different concentrations in the presence of H_2O_2 (20 μM). (g) Schematic diagram of Nano CO antibacterial.

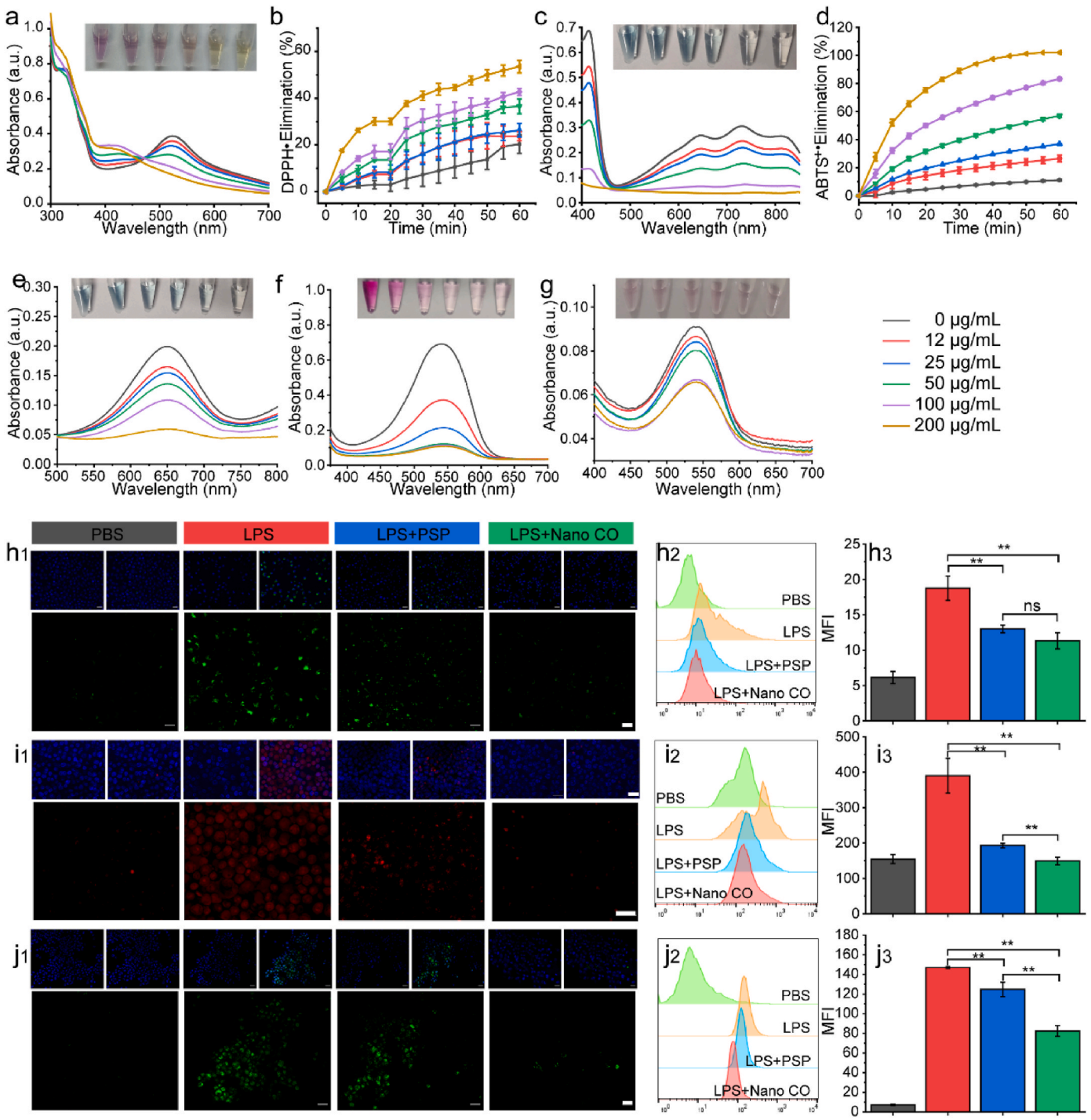

Fig. 3. RONS scavenging activity of Nano CO. (a) UV–vis absorbance spectra and (b) kinetic curves of DPPH• exposure to different concentrations of Nano CO. (c) UV–vis absorbance spectra and (d) kinetic curves of $ABTS^{+\bullet}$ exposure to different concentrations of Nano CO. (e–g) UV–vis absorbance spectra showing the radical eliminating activities of Nano CO for •OH (e), $\bullet O_2^-$ (f) and •NO (g), respectively. The concentrations of Nano CO are 200, 100, 50, 25, 12 μg/mL, respectively. (h–j) Fluorescence imaging (1), flow cytometry (2), and intensity quantification (3) showing the activities of PSP and Nano CO (200 μg/mL) to •OH (h), $\bullet O_2^-$ (i) and •NO (j) in RAW264.7 with LPS pretreatment. Scale bar = 40 μm. $^*p < 0.05$, $^{**}p < 0.01$, $^{***}p < 0.001$.

inconspicuous when it interacted with PSP (Fig. S5). Catalytic kinetics analysis demonstrated that Nano CO (200 μg/mL) removed 99.95% of the $ABTS^{+\bullet}$ within 60 min (Fig. 3d). These findings underscore the exceptional free radical scavenging ability and antioxidant capacity of Nano CO. Furthermore, we comprehensively studied its resistance to different physiologically related free radicals *in vitro*, including hydroxyl radicals (•OH), superoxide radicals ($\bullet O_2^-$), and nitric oxide (•NO). The ability of Nano CO to clear RONS was evaluated using the TMB probe for •OH, the superoxide anion kit for $\bullet O_2^-$ and the nitric oxide detection kit for •NO, respectively. As shown in Fig. 3e–g, the UV characteristic absorption peaks of these probes decreased in a concentration-dependent manner after incubation with Nano CO, confirming its broad-spectrum RONS elimination activity.

3.4. Intracellular RONS clearance and inhibition of RONS induced cell damage

RONS have emerged as pivotal factors in the pathophysiology of sepsis, where ROS such as •OH and $•O_2^-$ can cause DNA and mitochondrial damage, potentially leading to apoptosis. Concurrently, •NO plays a crucial role as an RNS in the septic cascade [34]. Therefore, managing intracellular RONS levels becomes crucial for controlling the onset and progression of sepsis. Inspired by its excellent antioxidant capacity *in vitro*, we proceeded to assess its antioxidant prowess at the cellular level. Initially, we evaluated the cytotoxicity of Nano CO and PSP in various cell types, including macrophages (RAW264.7), human microvascular endothelial cells (HMEC), human vascular smooth muscle cells (HVSMC) and human skin fibroblasts (HSF). As indicated in Fig. S6, even at concentrations as high as 200 μg/mL, both Nano CO and PSP exhibited no adverse effects on cell viability. These concentrations were subsequently chosen for further cellular experiments.

To investigate antioxidant activity, we pretreated RAW264.7 cells with LPS, a disease-associated molecular pattern known to activate the immune system, thereby creating a cellular model of sepsis that induces ROS overproduction and inflammation. After stimulating RAW264.7 cells with LPS for 24 h and co-incubated with Nano CO or PSP for another 24 h, the intracellular ROS level was then stained utilizing DCFH-DA for •OH, DHE for $•O_2^-$ and DAF-FM DA for NO, respectively, and further measured by fluorescence microscopy and flow cytometry (Fig. S7). As shown in Fig. 3h_1-j_1, intense green or red fluorescence was observed in LPS-stimulated cells, confirming the successful induction of cellular oxidative stress. After the addition of Nano CO or PSP (200 μg/mL), the fluorescence intensity in the cells significantly decreased, with the Nano CO group exhibiting more pronounced effects. Quantitative analysis using flow cytometry further substantiated that Nano CO significantly reduced intracellular RONS levels (Fig. 3h–j). To evaluate the broad antioxidant effects of Nano CO, we assessed its antioxidant capacity against four cell types, including RAW264.7, HMEC, HVSMC and HSF. As shown in Fig. S8, LPS-induced cells were marked green by the DCFH-DA probe, indicating oxidative stress within the cells. However, after Nano CO intervention, the intracellular green fluorescence disappeared, signifying the elimination of intracellular oxidative stress. Conversely, the removal efficacy of PSP was negligible. The above results indicated that Nano CO possesses broad-spectrum antioxidant activity.

Subsequently, we comprehensively evaluated the inhibitory effect of Nano CO on DNA damage, mitochondrial damage, and cell death caused by oxidative stress. As illustrated in the schematic diagram of Fig. 4a, ROS can induce the phosphorylation of the Ser139 site of histone variant H_2AX (γ-H_2AX), resulting in DNA double-strand breaks (DSBs). The protective effect of Nano CO on cellular DNA was assessed by detecting γ-H_2AX with DNA damage kit. As shown in Fig. 4b, both RAW264.7 and THP-1 (Human Acute Monocytic Leukemia Cells) stimulated by LPS exhibited intense green fluorescence, indicating severe DNA damage. In contrast, cells treated with Nano CO displayed weaker fluorescence signals compared to damaged cells, suggesting an inhibitory effect on DNA damage. Cells in the PSP group maintained strong fluorescence signals, indicating a limited repair ability. Additionally, we assessed mitochondrial damage by examining changes in mitochondrial membrane potential at sites of mitochondrial production in both cell types. The JC-1 fluorescent probe was used for mitochondrial membrane potential, emitting red fluorescence in active mitochondria with intact membrane potential and green fluorescence in mitochondria with reduced membrane potential. As depicted in Fig. 4c, LPS-stimulated cells displayed green fluorescence signals, revealing mitochondrial damage. The mitochondria showed limited recovery of red fluorescence following PSP treatment. Notably, Nano CO restored the quenched red fluorescence, demonstrating its effectiveness in combating oxidative stress and inhibiting mitochondrial damage. Furthermore, we employed the MitoSox ROS probe to specifically study the ability of Nano CO to clear mitochondrial fluorescence. As shown in Fig. S9, LPS-induced cells exhibited red fluorescence, indicating mitochondrial oxidative stress. Although the intervention with PSP did reduce the red fluorescence in damaged cell mitochondria, indicating a partial mitigation of oxidative stress, it was not completely eliminated. Nano CO intervention quenched the red fluorescence of mitochondria, indicating the reversal of mitochondrial oxidative stress. Therefore, the mechanism of action of Nano CO is universal in cells derived from different species. The next phase of our investigation delved into examining the protective capabilities of Nano CO against cell death induced by oxidative stress, utilizing H_2O_2 as ROS inducers. As presented in Fig. 4d, Nano CO exhibited a dose-dependent reduction in H_2O_2-induced cell death. These findings collectively indicate that Nano CO possesses the ability to scavenge intracellular ROS, preventing ROS-induced DNA and mitochondrial damage, along with preventing cell death. This approach holds potential significance by impeding ROS-related inflammatory cell signaling.

3.5. Anti-inflammatory effect of Nano CO in vitro

Given the robust anti-oxidative stress and organelle protection capabilities qualitied by CO, we sought to understand the underlying mechanisms. Acknowledging the heme oxygenase-1 (HO-1)/CO system as a cellular protection mechanism, we employed quantitative polymerase chain reaction (qPCR) and an HO-1 kit to assess the expression of HO-1 following various treatments. As depicted in Fig. 5a-b, both the mRNA and protein levels of HO-1 increased in LPS-stimulated macrophages, mainly due to compensatory increase. Notably, the presence of CO doubled the mRNA expression of HO-1, leading to a substantial increase in the corresponding protein levels. Similarly, THP-1 exhibited the same phenomenon after continuous intervention (Fig. S10). We further investigated the mechanism by which Nano CO triggers HO-1 expression. As depicted in Fig. 5c, Western blot (WB) experiments revealed that supplementing with exogenous Nano CO increased Nrf2 expression in a concentration-dependent manner, subsequently leading to the secretion of HO-1. These findings are consistent with previous research [35], highlighting the ability of exogenous CO to activate the intracellular HO-1/CO system. This activation enhances cellular resistance to oxidative stress-induced damage, thereby reducing the overall oxidative stress response.

Scientific investigations have established the inhibitory role of the HO-1/CO system in the NF-κB signaling pathway, thereby mitigating the inflammatory damage to tissue cells and suppressing the expression of inflammatory factors [18,36,37]. However, when infectious or non-infectious injury factors act on the body, damage-related molecular pattern activate toll-like receptor 4 (TLR-4) on the cell membrane. This activation initiates the nuclear NF-κB signaling pathway, mediating the release of inflammatory factors (NO, TNF-α, IL-6), further triggering an inflammatory cascade and leading to tissue and cell damage [38,39]. We proceeded to examine the expression of downstream inflammatory signals in activated macrophages following the activation of the HO-1 system. As exhibited in Fig. 5d–e, LPS-stimulated RAW264.7 showed increased mRNA levels of inducible nitric oxide synthase (iNOS) and released a significant amount of NO, leading to pronounced inflammation in the septic cell model. The intervention by PSP, which has weaker antioxidant activity, only partially reduced iNOS expression. Interestingly, there was no notable difference in mRNA levels of iNOS between actived cells treated with Nano CO and normal cells. Furthermore, the production of NO was effectively mitigated. Likewise, the levels of TNF-α and IL-6 released by inflammatory cells returned to normal levels after Nano CO intervention (Fig. 5f–g).

In another aspect, cell-free DNA (cfDNA), primarily originating from mitochondrial DNA and nuclear DNA released by damaged cells, is considered an crucial biomarker for sepsis prognosis and prediction [40]. cfDNA can be recognized by TLRs and induce intracellular signaling cascades, leading to the overexpression of inflammatory cytokines [40,41]. Therefore, scavenging cfDNA or blocking abnormal

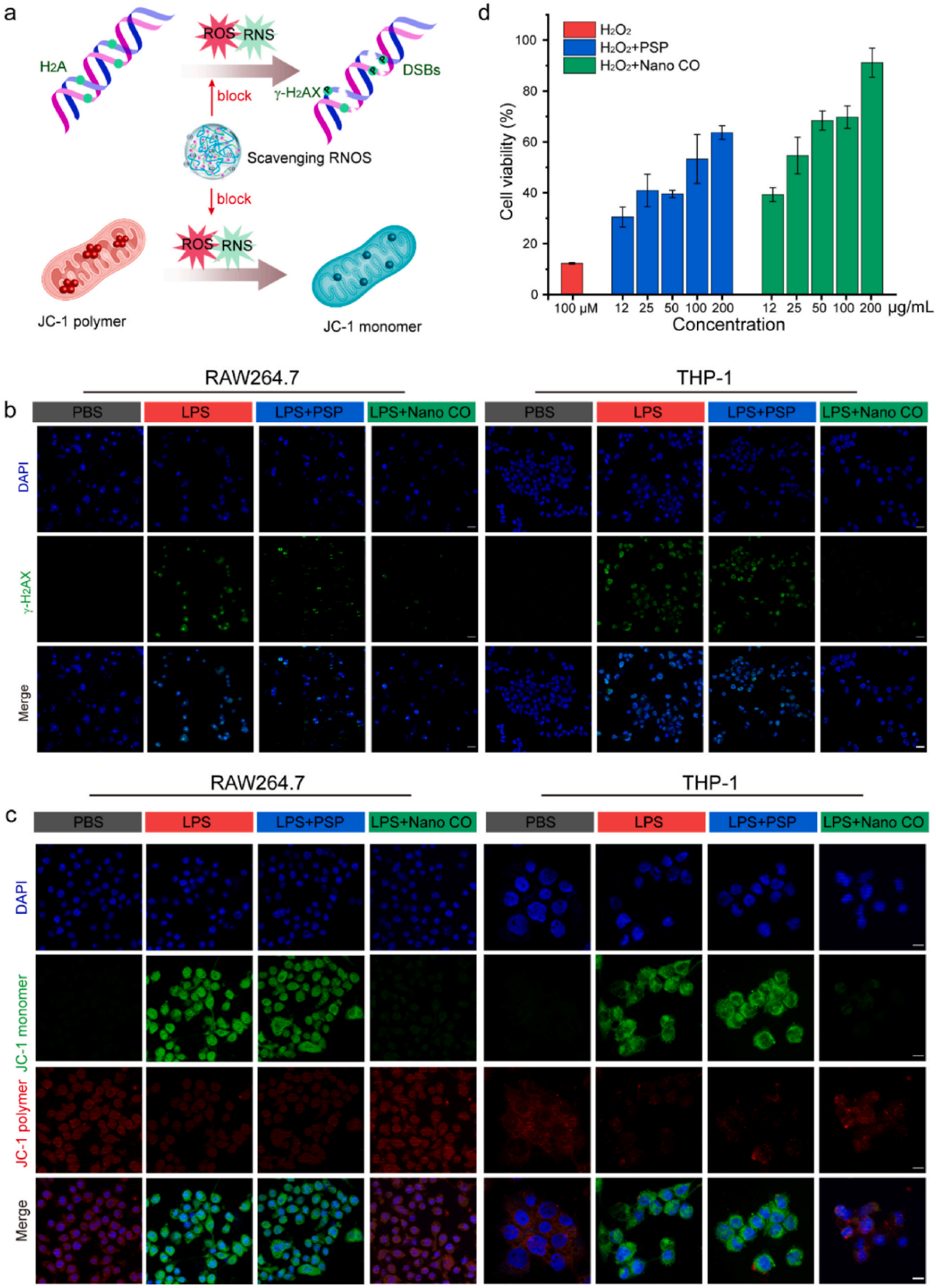

Fig. 4. Evaluation of Nano CO against cellular oxidative damage. (a) Schematic diagram of Nano CO against DNA and mitochondrial damage. (b) Phosphorylated histone variant γ-H_2AX imaging and (c) Mitochondrial membrane potential imaging of RAW264.7 and THP-1 following the treatments of PSP and Nano CO (200 μg/mL). Scale bar: 40 μm. (d) Protective effect of Nano CO on ROS-induced cell death. $^{*}p < 0.05$, $^{**}p < 0.01$, $^{***}p < 0.001$.

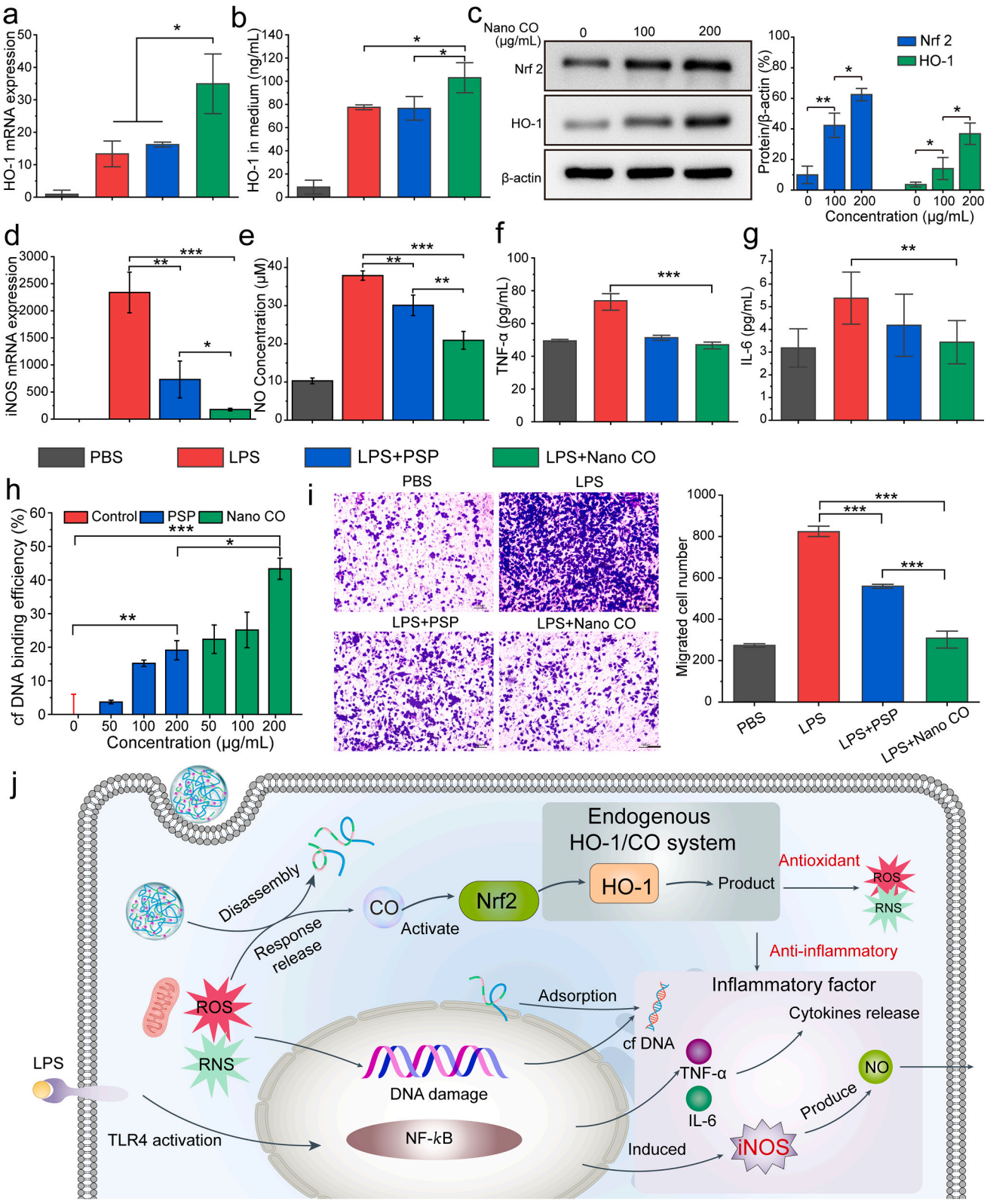

Fig. 5. Induction of HO-1 secretion and clearing inflammatory mediators. (a) HO-1 mRNA expression and (b) HO-1 concentration generated in RAW264.7 following the treatments of PSP and Nano CO (200 μg/mL), respectively. (c) WB analysis of Nrf2 and HO-1 expression in macrophages. WB shown are representative of three independent experiments. (d) iNOS mRNA expression, (e) NO concentration, (f) TNF-a and (g) IL-6 cytokine generated in macrophages following the treatments of PSP and Nano CO (200 μg/mL), respectively. (h) Binding affinity of PSP and Nano CO to cfDNA at different concentrations. (i) Representative images and quantitative analysis of macrophage migration induced by inhibition of activated macrophages. Scale bars: 100 μm. (j) Schematic diagram of anti-inflammatory effect of Nano CO. $^{*}p < 0.05$, $^{**}p < 0.01$, $^{***}p < 0.001$.

cfDNA pathways is anticipated to alleviate systemic inflammation in sepsis, consequently improving sepsis-induced organ damage. We further evaluated the binding affinity of Nano CO to cfDNA using the dsDNA HS Assay Kit. As illustrated in Fig. 5h, Nano CO exhibited a strong affinity for cfDNA in a dose-dependent manner. However, PSP also showed only weak binding to cfDNA. The above results may be attributed to the hydrogen bond between PEG and the phosphate backbone of DNA [34]. Subquently, we assessed the inflammatory potential of cfDNA after its adsorption by different materials. As depicted in Fig. S11, cfDNA was found to stimulate cells to release elevated levels of NO and TNF-α, thereby inducing cellular inflammation. However, the capacity of cfDNA to stimulate macrophages and trigger the secretion of inflammatory factors was markedly diminished after being adsorbed by PSP and Nano CO. Notably, Nano CO exhibited a more substantial reduction in the ability of cfDNA to induce inflammation. This confirms the effectiveness of Nano CO in adsorbing cfDNA and reducing the inflammatory response of host cells. Additionally, the accumulation of activated macrophages is known to exacerbate tissue inflammation [42]. We assessed the potential of Nano CO to decrease the recruitment of activated macrophages and alleviate tissue inflammation (Fig. S12). Surprisingly, LPS-stimulated macrophages induced chemotaxis by releasing attractants, leading to the recruitment of a large numbers of macrophages from the upper side to the lower side. However, Nano CO significantly reduced the migration ability of activated macrophages, indicating its capacity to inhibit macrophage recruitment and reduce inflammation (Fig. 5i). In summary, as shown in schematic Fig. 5j, Nano CO not only demonstrates anti-inflammatory properties by scavenging ROS, clearing cfDNA and alleviating cytokine release, but also by preventing macrophage migration induced by activated macrophages.

3.6. Inhibition of inflammation-induced pyroptosis

The excessive activation of pyroptosis significantly contribues to immune dysregulation in sepsis [12]. Pyroptosis, induced by canonical inflammasome such as NLRP3 or noncanonical inflammasome, plays a pivotal role in LPS-induced sepsis. This process involves the release of numerous cytokines through plasma membrane rupture, ultimately causing multiple organ damage and contributing to sepsis-related mortality [43]. The pyroptotic effector molecule Gasdermin D (GSDMD) is cleaved by inflammasome-activated caspase-1/-11 to generate an N-terminal fragment (GSDMD-NT). Subsequently, GSDMD-NT binds to the plasma membrane, oligomerizes, and forms membrane pores, leading to lytic cell death and the release of pro-inflammatory cytokines. At the same time, Caspase-1 can also process pro-IL-1β to form active IL-1β, Which is released extracellularly to amplify the inflammatory response [44–46]. Therefore, inhibiting or blocking pyroptosis represents a promising strategy to significantly improve survival and alleviate organ damage in LPS-induced sepsis.

Considering that Nano CO could activate the HO-1/CO system to alleviate the inflammatory cascade, we hypothesized that it might also block pyroptosis. To induce canonical inflammasomes or noncanonical inflammasomes, primary peritoneal macrophages were extracted from C57 mice and activated using ATP for caspase-1 induction, or LPS and Pam3CSK4 for caspase-11 induction, respectively. The successfully induced inflammatory macrophages were then co-cultured with PSP or Nano CO to evaluate the anti-pyroptosis ability. As shown in Fig. S13, pyroptosis was assessed by measuring lactate dehydrogenase (LDH) in the supernatant and propidium iodide (PI) uptake. LDH is a stable cytoplasmic enzyme that is released upon cell lysis, while PI is a small fluorescent molecule that binds to DNA through the damaged plasma membrane upon cell death. As expected, macrophages induced by ATP and LPS released substantial amounts of LDH, indicating successful pyroptosis induction (Fig. 6a–b). However, regardless of the two different cell pyroptosis modes, Nano CO effectively reduced LDH release in a concentration-dependent manner, whereas PSP exhibited a weaker inhibitory effect compared to Nano CO. Fluorescence imaging demonstrated that Nano CO could also reduce PI uptake, indicating its efficacy in preventing two different modes of pyroptosis (Fig. 6c–d).

Subsequently, we delved into the potential mechanism by which Nano CO inhibited pyroptosis through WB. As illustrated in Fig. 6e–f, macrophages neither underwent pyroptosis on their own nor under Nano CO stimulation (Lane 1 and 2). Both ATP and LPS caused the cleavage of GSDMD, yielding the GSDMD-NT band (Lane 3). Surprisingly, GSDMD-NT oligomers were weakened in both canonical and noncanonical inflammasome activation when treated with Nano CO (Lane 4). We then assessed intracellular IL-1β production and extracellular IL-1β release. The WB results revealed that inflammasome can induce IL-1β production (lane 3, Fig. S14a–b). However, after Nano CO intervention, intracellular IL-1β production markedly decreased (lane 4, Fig. S14a–b). Similarly, ELISA analysis demonstrated that pyroptosis increased IL-1β release, leading to an elevated supernatant concentration. Nonetheless, Nano CO intervention notably mitigated the IL-1β concentration in the cell supernatant (Figs. S14c–d). Hence, Nano CO can inhibit cell pyroptosis and prevent the expansion of inflammatory responses (Fig. 6g).

3.7. Induction of autophagy in macrophages

Autophagy, a natural protective mechanism of the body, plays a crucial role in maintaining internal environment stability. It not only inhibits excessive inflammation but also serves as an essential pathway for the body to combat pathogenic microorganisms [47,48]. In the advanced stages of sepsis, immunosuppression severely impairs autophagy, causing immune cell apoptosis and immune paralysis, which can have fatal effects on septic animals [49]. Therefore, we speculated that CO-induced HO-1 overexpression might promote autophagy to effectively alleviate tissue and organ damage. The autophagy status of primary macrophages following different treatments was observed through biological TEM images. As shown in Fig. 6h, whether under normal conditions or following Nano CO stimulation, the mitochondrial structure remained intact, demonstrating a normal autophagy state. However, there was evidence of mitochondrial swelling and reducted of autophagic vesicles in LPS-induced macrophages, indicating inhibited autophagy. Conversely, more autophagy vesicles and a relatively complete mitochondrial structure were observed in LPS-induced macrophages with the assistance of Nano CO. To further verify the promotion of autophagy, we used fluorescent staining to observe the autophagy status. Nano CO did not induce enhanced autophagy in healthy cells. However, in damaged cells where autophagy was inhibited, Nano CO reversed the inhibited state and enhance autophagy (Fig. S15). To further elucidate the role of autophagy activation, WB experiments were conducted to assess the levels of LC3 in primary macrophages treated with different conditions. The results indicated that Nano CO alone facilitated the conversion of LC3I to LC3II, demonstrating its capability to promote autophagy. Conversely, LPS hindered this transformation, signifying autophagy inhibition. Moreover, under inhibitory conditions, Nano CO fostered the conversion of LC3I to LC3II, reaffirming its role in promoting autophagy (Fig. 6i).

3.8. Biosafety evaluation of Nano CO in vivo

Firstly, we assessed the biosafety of Nano CO *in vivo*. Hemolysis experiments demonstrated that neither Nano CO nor PSP induced hemolysis of red blood cells (RBC), indicating their suitability for intravenous injection in mice (Fig. S16). Subsequently, we conducted a detailed analysis of blood CO concentration using a carbon monoxide hemoglobin detection kit to indirectly assess the release kinetics of Nano CO in both healthy and disease models. As depicted in Fig. S17, Nano CO gradually exhibited a release pattern in healthy mouse model, peaking in concentration within 24 h and returning to baseline levels by 96 h. Conversely, in the sepsis model characterized by oxidative stress, rapid release of Nano CO was observed, reaching its peak concentration within

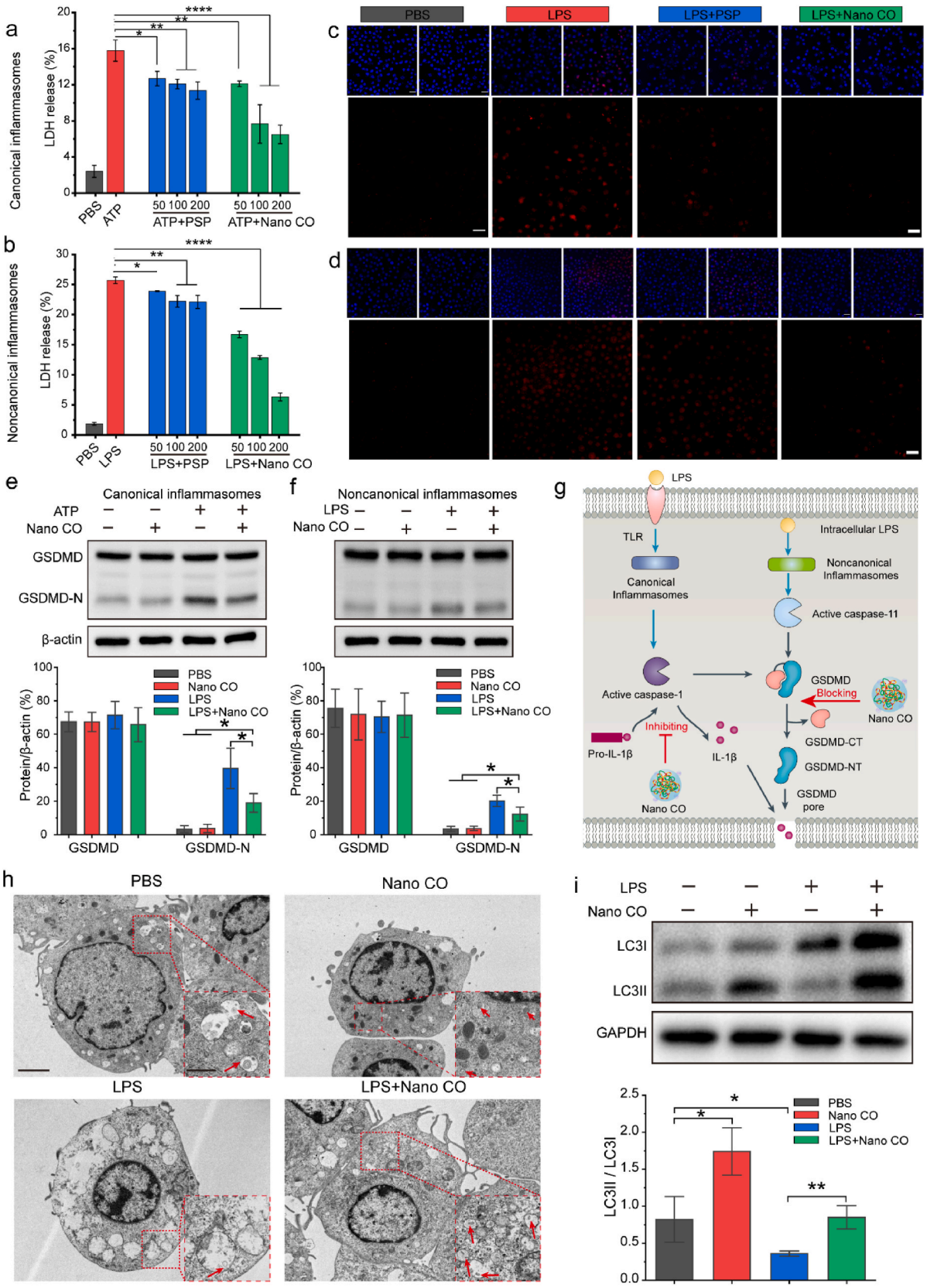

Fig. 6. Inhibition of pyroptosis and induction of autophagy. (a–b) LDH in supernatant of macrophages treated by increasing concentration of Nano CO and PSP (50, 100, 200 μg/mL) with stimulation of (a) canonical inflammasome or (b) noncanonical inflammasome, respectively. (c–d) Representative images of PI uptake in macrophages treated by Nano CO and PSP with stimulation of (c) canonical inflammasome or (d) noncanonical inflammasome, respectively. Scale bars: 40 μm. (e–f) WB and quantitative analysis of GSDMD markers of canonical and noncanonical inflammasome. (g) Schematic diagram of Nano CO inhibiting inflammation-induced pyroptosis. (h) Bio-TEM images of RAW264.7 cells after different treatments. Scale bars: 2 μm, 500 nm. (i) The expressions LC3-II/I in RAW264.7 cells after varied treatments. WB shown are representative of three independent experiments. $^{*}p < 0.05$, $^{**}p < 0.01$, $^{***}p < 0.001$.

6 h and returning to normal levels by 24 h. Next, healthy mice were intravenously injected with Nano CO (30 mg/kg), and serum samples were collected to measure biochemical indicators. According to Fig. S18, serum biochemical indicators showed no significant differences compared to healthy mice, suggesting no acute toxicity to the liver and kidneys. Hematoxylin-Eosin (H&E) staining of major organs (heart, liver, spleen, lung, and kidney) did not reveal any histopathological lesions (Fig. S19). In conclusion, Nano CO demonstrated high biocompatibility, making it a suitable nanomedicine for *in vivo* drug delivery.

3.9. Antisepsis therapeutic activity of Nano CO in LPS-induced sepsis model

Following this, we conducted intraperitoneal injections of varying doses of LPS into healthy mice to determine the half-lethal dose (LD50), clinical scores, survival rate, and body weight of the mice over 5 consecutive days. Clinical score and body temperature were important features of sepsis severity, directly reflecting the severity of sepsis and the damage caused by immune response to the body (Clinical scoring criteria are listed in the method section). Through assessment of these three key physiological parameters, it was observed that the mouse mortality rate reached 50% at an injection dose of 25 mg/kg, which was selected for further animal experiments (Fig. S20).

Next, we assayed the anti-septic therapeutic activity of Nano CO in an LPS-induced sepsis model. Following the established experimental protocol (Fig. 7a), we assessed the body weight, clinical score, and mortality of septic mice over 7 consecutive days after treatment with different regimens. Additionally, serum samples and major organs were collected 24 h post-treatment for pathological analysis. As illustrated in Fig. 7b, the clinical scores of septic mice treated with Nano CO or PSP were significantly reduced, pointing an improvement in the physical condition of the mice post-treatment. Initially, the survival rate of the mice was less than 30% due to the severe impact of prolonged sepsis. However, after treatment with Nano CO or PSP, the survival rates increased to 80% or 50%, respectively (Fig. 7c). LPS injection resulted in a rapid drop in the body temperature of the mice, while Nano CO treatment significantly alleviated the hypothermic effect associated with LPS intervention, denominating the ability of Nano CO to prevent sepsis-induced hypothermia (Fig. 7d). Furthermore, the surviving mice showed a gradual recovery in body weight post-treatment, indicating an improvement in their overall physical condition (Fig. S21). Moreover, we examined the efficacy of Nano CO in treating varying degrees of sepsis by assessing the survival rate. As shown in Fig. S22, under lethal dose conditions (30 mg/kg), the survival rate of mice with severe sepsis treated with CO increased to 30%. At the semi-lethal dose (25 mg/kg), the survival rate of mildly septic mice was maintained at 80%. These results indicated that Nano CO has a significant therapeutic effect on sepsis.

Given that multi-organ failure is a prevalent clinical manifestation of severe sepsis, we examined the potential for repairing multi-organ damage through histopathology. H&E staining images (Fig. 7e) showed that compared with PBS group, LPS induced extensive ballooning changes in the liver, accompanied by significant lung damage. Moreover, inflammatory cells infiltration was observed in the kidneys and spleen (marked by red arrows). After PSP treatment, there was partial restoration of organ functions in the mice, mainly manifested by reduced inflammatory cells presence in the kidney and spleen, although the lung and liver lesions were not effectively alleviated. Excitingly, after Nano CO treatment, the main organs of septic mice returned to normal state, with no inflammatory cell infiltration in the kidney and spleen, and there were no lesions in the liver and lungs. Furthermore, we collected serum for AST, AST, BUN and CRE test to evaluate the therapeutic impact on liver and kidney functions in different mice. As shown in Fig. S23, the liver and kidney functions of septic mice deteriorated significantly. Nevertheless, the liver and kidney functions of sepsis mice can be effectively restored after Nano CO treatment. These encouraging results suggested that Nano CO plays a role in restoring immune homeostasis in the body and alleviating multi-organ damage by clearing multiple inflammatory mediators in sepsis.

Next, we delved deeper into understanding the mechanisms behind the therapeutic effects of CO on sepsis. Specifically, we assessed the role of Nano CO in promoting HO-1 secretion and clearing multiple mediators of sepsis from the bloodstream. As illustrated in Fig. 8a, there was an increase in HO-1 expression in the serum of LPS-induced septic mice, primarily attributed to compensatory increase. Furthermore, exogenous CO stimulation amplified the secretion of HO-1 enzymes in septic mice, contributing to intracellular protective regulation and subsequent initiation of anti-inflammatory and antioxidant responses. Inflammatory mediators were significantly increased in the serum of septic mice, including NO, TNF-α and IL-6. The serum NO concentration of septic mice treated with Nano CO returned to normal levels, indicating that CO can effectively regulate inflammation in septic mice (Fig. 8b). Similarly, cytokine (TNF-α and IL-6) levels in treated mice also decreased synchronously compared with septic mice. However, septic mice treated with PSP had little effect on reducing inflammatory factors in the blood (Fig. 8c–d). Remarkably, a substantial amount of cfDNA was detected in mice with LPS-induced sepsis. PSP exhibited a capacity to adsorb cfDNA, resulting in a notable reduction in cfDNA concentration in mice. However, Nano CO treatment resulted in an even more significant decrease in cfDNA concentration compared to the PSP group. This reduction can be attributed not only to the adsorption capacity of cfDNA but also to the therapeutic effect of Nano CO in reducing the release of cfDNA during sepsis (Fig. 8e). Additionally, to evaluate the *in vivo* antioxidant effects of Nano CO, we measured the level of lipid peroxidation (MDA) and protein oxidative damage (protein carbonyls) in the serum of septic mice after different treatments. As illustrated in Fig. 8f, the MDA concentration in the serum of septic mice treated with Nano CO was significantly decreased compared to that of septic mice, nearly returning to normal levels. This normalization indicated a reduction in lipid peroxidation in the body, highlighting the antioxidant efficacy of Nano CO *in vivo*. Similarly, the protein carbonyl concentration, which reflects protein oxidative damage, also returned to normal levels (Fig. 8g). These experiments collectively proved that Nano CO could effectively remove various inflammatory mediators in the body and diminish the inflammatory cascade reaction.

Subsequently, we assessed bacterial burden, ROS level and activated macrophages in the peritoneal cavity. In mice treated with Nano CO, the peritoneal bacterial burden was significantly lower than that in septic mice, approaching levels observed in healthy subjects (Fig. 8h–i). Compared to the LPS-septic mice group, Nano CO-treated mice showed a reduction in the proportion of peritoneal cells with high ROS levels (Fig. 8j–k), indicating an improvement in the peritoneal inflammatory environment. Simultaneously, the proportion of peritoneal M1-polarized macrophages decreased in Nano CO treated mice, affirming the hindrance of macrophage activation (Fig. 8l-m). The aforementioned results illustrated that treatment with Nano CO gradually restored the inflammatory storm and immune system to normal levels in septic mice, confirming that Nano CO is an ideal treatment for sepsis.

Moreover, we selected the liver and lung, which exhibited more severe lesions, as representative organs to investigate the expression of HO-1 through immunofluorescence. As anticipated, LPS triggered a compensatory increase in HO-1 expression in organs (Fig. 8n). Remarkably, exogenous CO intervention further enhanced the expression of HO-1. Given the HO-1 increasing capacity, we conducted immunofluorescence staining to assess ROS levels in internal organs. As demonstrated in Fig. S24, there was a substantial increase in ROS levels within the internal organs of septic mice. However, post Nano CO treatment, ROS levels in Nano CO-treated mice significantly decreased, suggesting that CO treatment contributed to the amelioration of organ oxidative stress. These combined results affirm that CO administration elicits antioxidant effects in mice, resulting in a marked reduction in oxidative damage among septic mice. Subsequently, we explored the

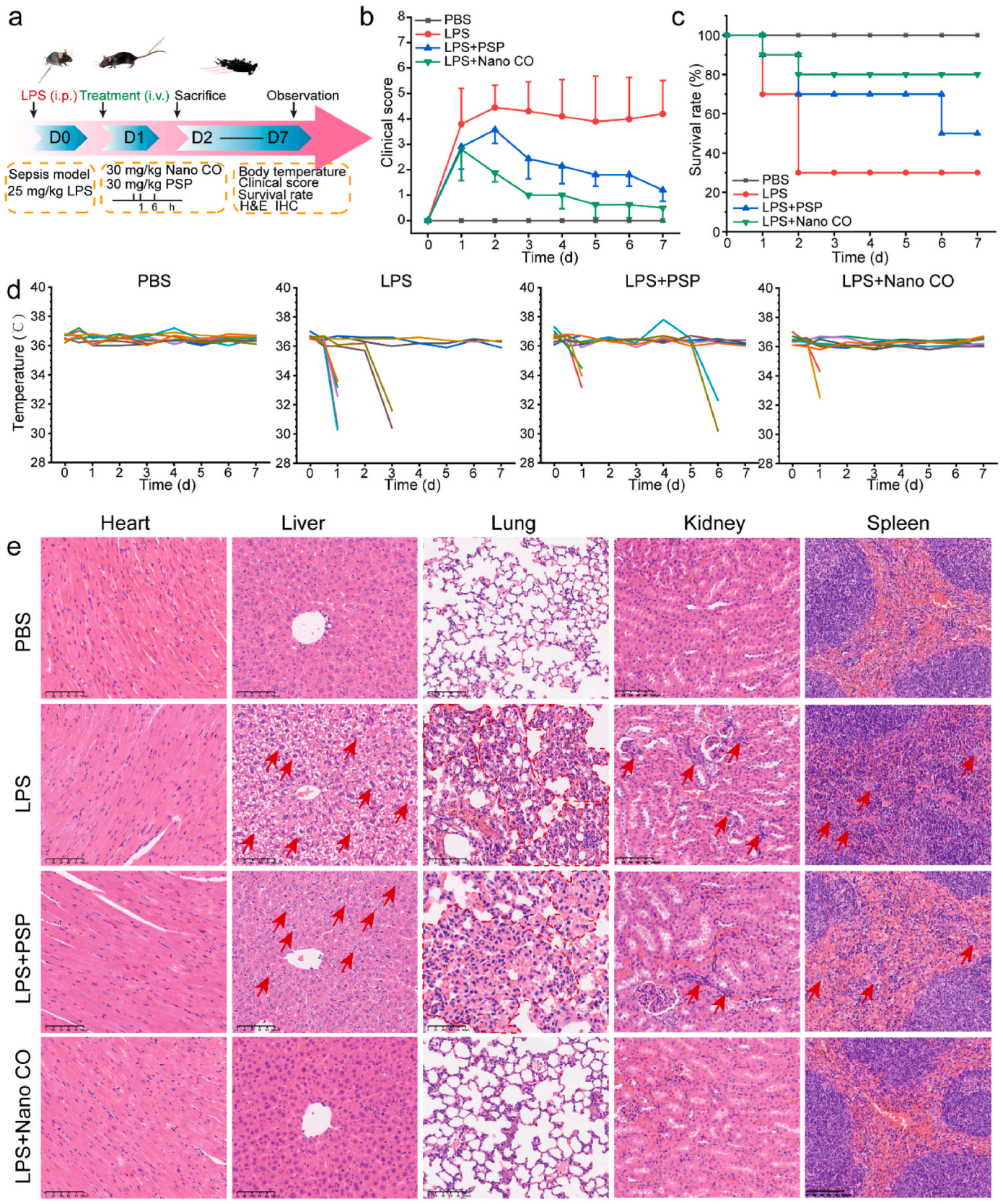

Fig. 7. Therapeutic effect of Nano CO on LPS-induced sepsis. (a) Schematic diagram of animal experiment schedule. (b) Clinical score, (c) survival rate and (d) body temperature of mice in different treatment groups recorded for seven consecutive days, respectively. (e) H&E Staining of mice in different treatment groups. Scale bars: 100 μm.

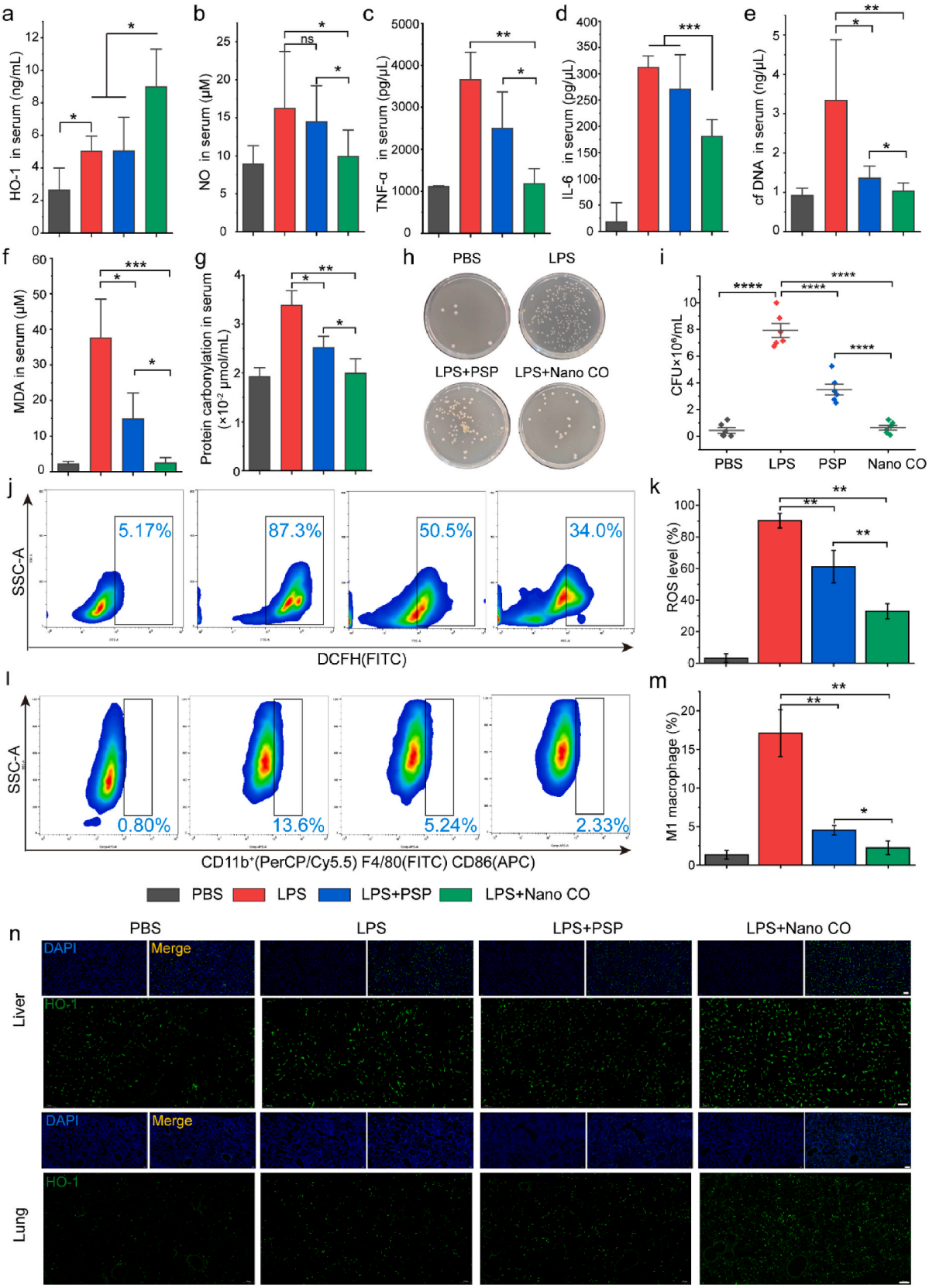

Fig. 8. Effect on multiple meditators of sepsis *in vivo*. (a) HO-1, (b) NO, (c) TNF-α, (d) IL-6, (e) cfDNA, (f) MDA and (g) protein carbonylation in serum of mice after different treatment. (g) Bacterial colony image and (i) bacteria burden from peritoneal cavity of mice in different treatment groups. (j) Flow cytometry and (k) intensity quantification exhibiting with ROS level in peritoneal cells following different treatment. (l) Flow cytometry and (m) intensity quantification exhibiting M1 polarization ratio of macrophages following different treatment. (n) Representative images of HO-1 immunofluorescence staining in liver and lung. Scale bars: 100 μm. $^{*}p < 0.05$, $^{**}p < 0.01$, $^{***}p < 0.001$.

oxidative protection of nanoparticles in liver and lung by detecting DNA damage. As shown in Fig. S25, the injection of Nano CO reversed the LPS induced DNA damage in tissues. These results indicated that Nano CO had potential in scavenging ROS *in vivo*, protecting the body from oxidative damage. Furthermore, we evaluated the expression of TNF-α and IL-6 cytokines in the organs (Fig. S26–S27). Under LPS induction, the levels of cytokines in liver and lung were abundant, indicating the occurrence of an inflammatory storm in the mice. Notably, the levels of cytokines in septic mice treated with Nano CO decreased deeply, illustrating the reversal of the inflammatory response. However, PSP intervention did not yield significant improvements in tissue inflammation levels. Furthermore, inflammation triggered severe pyroptosis in the internal organs of septic mice, exacerbating the inflammatory response and causing severe lesions (Fig. S28). Nano CO intervention effectively suppressed pyroptosis and ameliorated inflammation levels. As anticipated, autophagy was significantly suppressed in septic mouse organs. Nevertheless, Nano CO treatment effectively promoted autophagy, contributing to reduced inflammation (Fig. S29). In conclusion, Nano CO improved sepsis survival rate by scavenging RONS and cfNDA, activating HO-1 system, reducing pro-inflammatory cytokines, inhibiting pyroptosis, and activating autophagy, exhibiting extensive therapeutic benefits in sepsis models.

4. Conclusion

The heightened mortality and unfavorable treatment prognosis associated with sepsis have prompted increased attention towards the development of novel drugs in this field. The primary contributing factor may be linked to immune dysregulation in affected patients. Therefore, this study aims to alleviating the inflammatory storm of sepsis by removing inflammatory mediators and activing intracellular self-protection system. Given the cytoprotective and homeostatic properties of CO, it is hypothesized to play a pivotal role in immune regulation in sepsis. However, the challenges of transforming it into an injectable drug with a controllable dose supply have impeded its widespread application. In this investigation, we employed nano-self-assembly technology to graft metal carbonyl compounds onto polymers to form water-soluble nanodrugs (Nano CO). These nanodrugs can selectively release CO in response to the ROS environment, offering a controlled approach for the injectable treatment of sepsis. Nano CO exhibited notable efficacy in eliminating various sepsis mediators by binding to cfDNA, removing harmful RONS and bacteria, blocking macrophage activation, inhibiting pyroptosis and activating autophagy, thereby alleviating the inflammatory storm. Experimental findings demonstrated good *in vivo* biocompatibility of Nano CO, and increased the survival rate of mice with sepsis up to 80%. Pathological assessments revealed that Nano CO significantly alleviated systemic inflammation, mitigated organ failure, and provided robust protection in sepsis models. Convincingly, the strategy of scavenging or targeting multiple inflammatory mediators with multifunctional Nano CO provided a promising avenue for the development of effective treatments for sepsis as well as many other inflammation-related diseases.

Developing strategies to minimize potential toxic effects is a key focus in the development of new drugs. While we have confirmed the biological safety of Nano CO at specific doses, it's essential to recognize that all substances, including CO, can become toxic beyond certain thresholds. Apart from investigating the protective effects of CO against organ damage, it's imperative to thoroughly explore its potential side effects from metabolic and toxicological perspectives. CO, whether administered as a gas or through a carrier, has demonstrated beneficial effects in animal disease models. However, it encounters numerous challenges during clinical trials, including safety concerns, distribution issues, and metabolic considerations. Although CO may appear as a hazardous gas, it's crucial to acknowledge its potential therapeutic applications without underestimating them. At the very least, the simplicity of CO will continue to lead to intriguing new avenues of research as we delve deeper into the intricacies of cellular processes.

Declaration of competing interest

The authors declare that they have no known competing financial interests or personal relationships that could have appeared to influence the work reported in this paper.

Data availability statement

Data will be made available on request.

Ethics approval

All animal-related operations in this work were approved by Animal Experimental Ethical Inspection of Laboratory Animal Centre, Huazhong Agriculture University (ID number: HZAUMO-2023-0197).

CRediT authorship contribution statement

Yang Wu: Writing – original draft, Visualization, Methodology, Conceptualization. **Xia Chen:** Visualization, Methodology, Investigation. **Zhaolin Zeng:** Investigation. **Bei Chen:** Investigation. **Zhenxing Wang:** Investigation. **Zhiyong Song:** Investigation. **Hui Xie:** Writing – review & editing, Writing – original draft, Supervision, Conceptualization.

Acknowledgments

This research was supported by National Natural Science Foundation of China (Grant No. 82302720 to Y.Wu; 82125023, 82072504 to H. Xie; 82272562 to Z-X Wang), Natural Science Foundation of Hunan Province (Grant No. 2023JJ40997 to Y. Wu), China Postdoctoral Science Foundation (Grant No. 2023M733964 to Y. Wu, 2023M733946 to X. Chen).

Appendix A. Supplementary data

Supplementary data to this article can be found online at https://doi.org/10.1016/j.bioactmat.2024.04.013.

References

[1] C. Lelubre, J.L. Vincent, Mechanisms and treatment of organ failure in sepsis, Nat. Rev. Nephrol. 14 (7) (2018) 417–427.
[2] M. Huang, S. Cai, J. Su, The pathogenesis of sepsis and potential therapeutic targets, Int. J. Mol. Sci. 20 (21) (2019) 5376.
[3] W.H. Organization, Global report on the epidemiology and burden of sepsis. https://www.sccm.org/getattachment/SurvivingSepsisCampaign/Gudelines/Adult-Patients/Surviving-SepsisCampaign-Hour-1-Bundle, 2020.
[4] T. van der Poll, M. Shankar-Hari, W.J. Wiersinga, The immunology of sepsis, Immunity 54 (11) (2021) 2450–2464.
[5] J.M. Cavaillon, M. Singer, T. Skirecki, Sepsis therapies: learning from 30 years of failure of translational research to propose new leads, EMBO Mol. Med. 12 (4) (2020) e10128.
[6] K.E. Rudd, S.C. Johnson, K.M. Agesa, K.A. Shackelford, D. Tsoi, D.R. Kievlan, D. V. Colombara, K.S. Ikuta, N. Kissoon, S. Finfer, Global, regional, and national sepsis incidence and mortality, 1990-2017: analysis for the global burden of disease study, Lancet 395 (10219) (2020) 200–211.
[7] D. Rittirsch, M.A. Flierl, P.A. Ward, Harmful molecular mechanisms in sepsis, Nat. Rev. Immunol. 8 (10) (2008) 776–787.
[8] F. Cao, L. Zhang, Y. You, L. Zheng, J. Ren, X. Qu, An enzyme-mimicking single-atom catalyst as an efficient multiple reactive oxygen and nitrogen species scavenger for sepsis management, Angew. Chem. Int. Ed. 132 (13) (2020) 5146–5153.
[9] N.L. Haddock, L.J. Barkal, N. Ram-Mohan, G. Kaber, C.Y. Chiu, A.S. Bhatt, S. Yang, P.L. Bollyky, Phage diversity in cell-free DNA identifies bacterial pathogens in human sepsis cases, Nat. Microbiol. 8 (2023) 1495–1507.
[10] F. Venet, G. Monneret, Advances in the understanding and treatment of sepsis-induced immunosuppression, Nat. Rev. Nephrol. 14 (2) (2017) 121–127.
[11] X. Liu, S. Xia, Z. Zhang, H. Wu, J. Lieberman, Channelling inflammation: gasdermins in physiology and disease, Nat. Rev. Drug Discov. 20 (5) (2021) 384–405.

[12] J.J. Hu, X. Liu, S. Xia, Z. Zhang, Y. Zhang, J. Zhao, J. Ruan, X. Luo, X. Lou, Y. Bai, FDA-approved disulfiram inhibits pyroptosis by blocking gasdermin D pore formation, Nat. Immunol. 21 (7) (2020) 736–745.
[13] D.D. Zhu, Y.L. Huang, S.Y. Guo, N. Li, X.W. Yang, A.R. Sui, Q. Wu, Y. Zhang, Y. Kong, Q.F. Li, AQP4 aggravates cognitive impairment in sepsis-associated encephalopathy through inhibiting Na_v1. 6-mediated astrocyte autophagy, Adv. Sci. 10 (14) (2023) 2205862.
[14] L. Yu, P. Hu, Y. Chen, Gas-generating nanoplatforms: material chemistry, multifunctionality, and gas therapy, Adv. Mater. 30 (49) (2018) 1801964.
[15] S.G. allego, G.J.L. Bernardes, Carbon-monoxide-releasing molecules for the delivery of therapeutic CO in vivo, Angew. Chem. Int. Ed. 53 (37) (2015) 9712–9721.
[16] Z. Xia, C. Zhang, C. Guo, B. Song, W. Hu, Y. Cui, Y. Xue, M. Xia, D. Xu, S. Zhang, J. Fang, Nanoformulation of a carbon monoxide releasing molecule protects against cyclosporin a-induced nephrotoxicity and renal fibrosis via the suppression of the NLRP3 inflammasome mediated TGF-β/smad pathway, Acta Biomater. 144 (2022) 42–53.
[17] N.K. Campbell, H.K. Fitzgerald, A. Dunne, Regulation of inflammation by the antioxidant haem oxygenase 1, Nat. Rev. Immunol. 21 (7) (2021) 411–425.
[18] S.W. Ryter, Therapeutic potential of heme oxygenase-1 and carbon monoxide in acute organ injury, critical illness, and inflammatory disorders, Antioxidants 9 (11) (2020) 1153.
[19] Y. Cui, C. Guo, Z. Xia, Y. Xue, B. Song, W. Hu, X. He, S. Liang, Y. Wei, C. Zhang, H. Wang, D. Xu, S. Zhang, J. Fang, Exploring the therapeutic potential of a nano micelle containing a carbon monoxide-releasing molecule for metabolic-associated fatty liver disease by modulating hypoxia-inducible factor-1α, Acta Biomater. 169 (2023) 500–516.
[20] X. Ji, C. Zhou, K. Ji, R.E. Aghoghovbia, Z. Pan, V. Chittavong, B. Ke, B. Wang, Click and release: a chemical strategy toward developing gasotransmitter prodrugs by using an intramolecular Diels-Alder reaction, Angew. Chem. Int. Ed. 55 (51) (2016) 15846–15851.
[21] K. Magierowska, M. Magierowski, CO in gastrointestinal physiology and protection, carbon monoxide in drug discovery: basics, Pharmacology, and Therapeutic Potential (2022) 466–481.
[22] B. Song, C. Zhang, W. Hu, C. Guo, Z. Xia, W. Hu, M. Qin, W. Jiang, J. Lv, D. Xu, S. Zhang, J. Fang, Nano-designed carbon monoxide donor SMA/CORM2 exhibits protective effect against acetaminophen induced liver injury through macrophage reprograming and promoting liver regeneration, J. Contr. Release 331 (2021) 350–363.
[23] E. Korbut, T. Brzozowski, M. Magierowski, Carbon monoxide being hydrogen sulfide and nitric oxide molecular sibling, as endogenous and exogenous modulator of oxidative stress and antioxidative mechanisms in the digestive system, Oxid. Med. Cell. Longev. 2020 (2020) 1–12.
[24] R. Motterlini, L.E. Otterbein, The therapeutic potential of carbon monoxide, Nat. Rev. Drug Discov. 9 (9) (2010) 728–743.
[25] H. Yin, J. Fang, L. Liao, H. Nakamura, H. Maeda, Styrene-maleic acid copolymer-encapsulated CORM2, a water-soluble carbon monoxide (CO) donor with a constant CO-releasing property, exhibits therapeutic potential for inflammatory bowel disease, J. Contr. Release 187 (2014) 14–21.
[26] C. Guo, C. Zhang, Z. Xia, B. Song, W. Hu, Y. Cui, Y. Xue, M. Xia, D. Xu, S. Zhang, J. Fang, Nano-designed CO donor ameliorates bleomycin-induced pulmonary fibrosis via macrophage manipulation, J. Contr. Release 341 (2022) 566–577.
[27] G. Toda, T. Yamauchi, T. Kadowaki, K. Ueki, Preparation and culture of bone marrow-derived macrophages from mice for functional analysis, STAR Protocols 2 (1) (2021).
[28] Q. Cai, J. Jiang, H. Zhang, P. Ge, L. Yang, W. Zhu, Reduction-responsive anticancer nanodrug using a full poly(ethylene glycol) carrier, ACS Appl. Mater. Interfaces 13 (16) (2021) 19387–19397.
[29] W. Jiang, W. Dong, M. Li, Z. Guo, Q. Wang, Y. Liu, Y. Bi, H. Zhou, Y. Wang, Nitric oxide induces immunogenic cell death and potentiates cancer immunotherapy, ACS Nano 16 (3) (2022) 3881–3894.
[30] G. Ma, Z. Liu, C. Zhu, H. Chen, R.T.K. Kwok, P. Zhang, B.Z. Tang, L. Cai, P. Gong, H_2O_2-responsive NIR-II AIE nanobomb for carbon monoxide boosting low-temperature photothermal therapy, Angew. Chem. Int. Ed. 61 (36) (2022) e202207213.
[31] J. Meng, Z. Jin, P. Zhao, B. Zhao, M. Fan, Q. He, A multistage assembly/disassembly strategy for tumor-targeted CO delivery, Sci. Adv. 6 (20) (2020) eaba1362.
[32] D. Wu, X. Duan, Q. Guan, J. Liu, X. Yang, F. Zhang, P. Huang, J. Shen, X. Shuai, Z. Cao, Mesoporous polydopamine carrying manganese carbonyl responds to tumor microenvironment for multimodal imaging-guided cancer therapy, Adv. Funct. Mater. 29 (16) (2019) 1900095.
[33] Q. He, D.O. Kiesewetter, Y. Qu, X. Fu, J. Fan, P. Huang, Y. Liu, G. Zhu, Y. Liu, Z. Qian, NIR-responsive on-demand release of CO from metal carbonyl-caged graphene oxide nanomedicine, Adv. Mater. 27 (42) (2015) 6741.
[34] F. Liu, S. Sheng, D. Shao, Y. Xiao, Y. Zhong, J. Zhou, C.H. Quek, Y. Wang, J. Dawulieti, C. Yang, H. Tian, X. Chen, K.W. Leong, Targeting multiple mediators of sepsis using multifunctional tannic acid-Zn^{2+}-gentamicin nanoparticles, Matter 4 (11) (2021) 3677–3695.
[35] K.M. Kim, H.O. Pae, M. Zheng, R. Park, Y.M. Kim, H.T. Chung, Carbon monoxide induces heme oxygenase-1 via activation of protein kinase R-like endoplasmic reticulum kinase and inhibits endothelial cell apoptosis triggered by endoplasmic reticulum stress, Circ. Res. 101 (9) (2007) 919–927.
[36] A. Hedblom, S.M. Hejazi, G. Canesin, R. Choudhury, K.A. Hanafy, E. Csizmadia, J. L. Persson, B. Wegiel, Heme detoxification by heme oxygenase-1 reinstates proliferative and immune balances upon genotoxic tissue injury, Cell Death Dis. 10 (2) (2019) 72.
[37] Y. Xue, D. Zhang, Y. Wei, C. Guo, B. Song, Y. Cui, C. Zhang, D. Xu, S. Zhang, J. Fang, Polymeric nano-micelle of carbon monoxide donor SMA/CORM2 ameliorates acetaminophen-induced liver injury via suppressing HMGB1/TLR4 signaling pathway, Eur. J. Pharmaceut. Sci. 184 (2023).
[38] Y.Y. Zhang, B.T. Ning, Signaling pathways and intervention therapies in sepsis, Signal Transduct. Targeted Ther. 6 (1) (2021) 407.
[39] S. Kassirian, R. Taneja, S. Mehta, Diagnosis and management of acute respiratory distress syndrome in a time of Covid-19, Diagnostics 10 (12) (2020) 1053.
[40] Q. Jing, C.H.C. Leung, A.R. Wu, Cell-free DNA as biomarker for sepsis by integration of microbial and host information, Clin. Chem. 68 (9) (2022) 1184–1195.
[41] H. Zhu, B. Kong, J. Che, Y. Zhao, L. Sun, Bioinspired nanogels as cell-free DNA trapping and scavenging organelles for rheumatoid arthritis treatment, Proc. Natl. Acad. Sci. USA 120 (33) (2023) e2303385120.
[42] J. Guo, D. Li, H. Tao, G. Li, R. Liu, Y. Dou, T. Jin, L. Li, J. Huang, H. Hu, J. Zhang, Cyclodextrin-derived intrinsically bioactive nanoparticles for treatment of acute and chronic inflammatory diseases, Adv. Mater. 31 (46) (2019) 1904607.
[43] X. Liu, S. Xia, Z. Zhang, H. Wu, J. Lieberman, Channelling inflammation: gasdermins in physiology and disease, Nat. Rev. Drug Discov. 20 (5) (2021) 384–405.
[44] T. Bergsbaken, S.L. Fink, B.T. Cookson, Pyroptosis: host cell death and inflammation, Nat. Rev. Microbiol. 7 (2) (2009) 99–109.
[45] W. Gao, X. Wang, Y. Zhou, X. Wang, Y. Yu, Autophagy, ferroptosis, pyroptosis, and necroptosis in tumor immunotherapy, Signal Transduct. Targeted Ther. 7 (1) (2022) 196.
[46] P. Devant, J.C. Kagan, Molecular mechanisms of gasdermin D pore-forming activity, Nat. Immunol. 24 (7) (2023) 1064–1075.
[47] K. Nakahira, J.A. Haspel, V.A. Rathinam, S.J. Lee, T. Dolinay, H.C. Lam, J. A. Englert, M. Rabinovitch, M. Cernadas, H.P. Kim, Autophagy proteins regulate innate immune responses by inhibiting the release of mitochondrial DNA mediated by the NALP3 inflammasome, Nat. Immunol. 12 (3) (2011) 222–230.
[48] J.N.S. Vargas, M. Hamasaki, T. Kawabata, R.J. Youle, T. Yoshimori, The mechanisms and roles of selective autophagy in mammals, Nat. Rev. Mol. Cell Biol. 24 (3) (2022) 167–185.
[49] J. Ho, J. Yu, S.H. Wong, L. Zhang, X. Liu, W.T. Wong, C.C. Leung, G. Choi, M. H. Wang, T. Gin, Autophagy in sepsis: degradation into exhaustion? Autophagy 12 (7) (2016) 1073–1082.